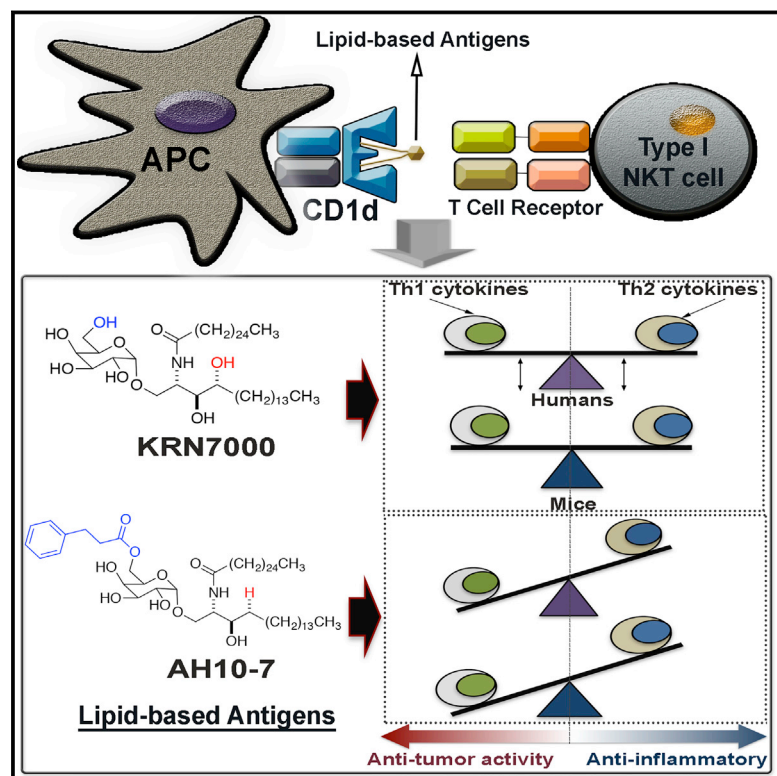


# Cell Chemical Biology

## Dual Modifications of $\alpha$ -Galactosylceramide Synergize to Promote Activation of Human Invariant Natural Killer T Cells and Stimulate Anti-tumor Immunity

### Graphical Abstract



### Authors

Divya Chennamadhavuni,  
Noemi Alejandra Saavedra-Avila,  
Leandro J. Carreño, ...,  
Jérôme Le Nours, Steven A. Porcelli,  
Amy R. Howell

### Correspondence

jerome.lenours@monash.edu (J.L.N.),  
steven.porcelli@einstein.yu.edu (S.A.P.),  
amy.howell@uconn.edu (A.R.H.)

### In Brief

Chennamadhavuni et al. synthesized an improved activating ligand for *i*NKT cells by combining carbohydrate and sphingoid base modifications in an  $\alpha$ -galactosyl ceramide. Biological and structural studies provide insight into the mechanisms responsible for improved activity and suggest approaches for further optimization of ligand design.

### Highlights

- Sphinganine  $\alpha$ -galactosylceramides strongly activate mouse but not human *i*NKT cells
- A modification of galactose is described that restores human *i*NKT cell responses
- The modified  $\alpha$ -GalCer retains improved proinflammatory and anti-tumor properties
- Crystallography and molecular modeling provide mechanistic insight into bioactivity



# Dual Modifications of $\alpha$ -Galactosylceramide Synergize to Promote Activation of Human Invariant Natural Killer T Cells and Stimulate Anti-tumor Immunity

Divya Chennamadhavuni,<sup>1,11</sup> Noemi Alejandra Saavedra-Avila,<sup>2,11</sup> Leandro J. Carreño,<sup>2,10</sup> Matthew J. Guberman-Pfeffer,<sup>1</sup> Pooja Arora,<sup>2</sup> Tang Yongqing,<sup>4,5</sup> Hui-Fern Koay,<sup>6</sup> Dale I. Godfrey,<sup>6,7</sup> Santosh Keshipeddy,<sup>1</sup> Stewart K. Richardson,<sup>1</sup> Srinivasan Sundararaj,<sup>4,5</sup> Jae Ho Lo,<sup>8</sup> Xiangshu Wen,<sup>8</sup> José A. Gascón,<sup>1</sup> Weiming Yuan,<sup>8</sup> Jamie Rossjohn,<sup>4,5,9</sup> Jérôme Le Nours,<sup>4,5,\*</sup> Steven A. Porcelli,<sup>2,3,\*</sup> and Amy R. Howell<sup>1,12,\*</sup>

<sup>1</sup>Department of Chemistry, The University of Connecticut, Storrs, CT 06269-3060, USA

<sup>2</sup>Department of Microbiology and Immunology, Albert Einstein College of Medicine, Bronx, NY 10461, USA

<sup>3</sup>Department of Medicine, Albert Einstein College of Medicine, Bronx, NY 10461, USA

<sup>4</sup>Infection and Immunity Program, Department of Biochemistry and Molecular Biology, Biomedicine Discovery Institute, Monash University, Clayton, VIC 3800, Australia

<sup>5</sup>Australian Research Council Centre of Excellence for Advanced Molecular Imaging, Monash University, Clayton, VIC 3800, Australia

<sup>6</sup>Department of Microbiology & Immunology, Peter Doherty Institute for Infection and Immunity, University of Melbourne, Melbourne, Australia

<sup>7</sup>Australian Research Council Centre of Excellence for Advanced Molecular Imaging at the University of Melbourne, Melbourne, Australia

<sup>8</sup>Department of Molecular Microbiology and Immunology, Keck School of Medicine, University of Southern California, Los Angeles, CA 90033, USA

<sup>9</sup>Institute of Infection and Immunity, Cardiff University, School of Medicine, Heath Park, Cardiff CF14 4XN, UK

<sup>10</sup>Millennium Institute on Immunology and Immunotherapy, Programa de Inmunología, Instituto de Ciencias Biomédicas, Facultad de Medicina, Universidad de Chile, Santiago, Chile

<sup>11</sup>These authors contributed equally

<sup>12</sup>Lead Contact

\*Correspondence: [jerome.lenours@monash.edu](mailto:jerome.lenours@monash.edu) (J.L.N.), [steven.porcelli@einstein.yu.edu](mailto:steven.porcelli@einstein.yu.edu) (S.A.P.), [amy.howell@uconn.edu](mailto:amy.howell@uconn.edu) (A.R.H.)  
<https://doi.org/10.1016/j.chembiol.2018.02.009>

## SUMMARY

Glycosylceramides that activate CD1d-restricted invariant natural killer T (*i*NKT) cells have potential therapeutic applications for augmenting immune responses against cancer and infections. Previous studies using mouse models identified sphinganine variants of  $\alpha$ -galactosylceramide as promising *i*NKT cell activators that stimulate cytokine responses with a strongly proinflammatory bias. However, the activities of sphinganine variants in mice have generally not translated well to studies of human *i*NKT cell responses. Here, we show that strongly proinflammatory and anti-tumor *i*NKT cell responses were achieved in mice by a variant of  $\alpha$ -galactosylceramide that combines a sphinganine base with a hydrocinnamoyl ester on C6'' of the sugar. Importantly, the activities observed with this variant were largely preserved for human *i*NKT cell responses. Structural and *in silico* modeling studies provided a mechanistic basis for these findings and suggested basic principles for capturing useful properties of sphinganine analogs of synthetic *i*NKT cell activators in the design of immunotherapeutic agents.

## INTRODUCTION

Invariant natural killer T (*i*NKT) cells are a subset of unconventional T cells that participate in both adaptive and innate

immunity (Bendelac et al., 2007; Brennan et al., 2013). A major feature that sets them apart from conventional T cells, which recognize peptides presented by major histocompatibility complex (MHC) molecules, is their recognition of lipid-based antigens presented by the MHC class I-like CD1d protein (Rossjohn et al., 2012). Since the discovery over two decades ago that natural forms of  $\alpha$ -galactosylceramide ( $\alpha$ -GalCer) known as agelasphins and their synthetic analogs are potent stimulators of *i*NKT cell responses with anti-cancer activities (Kawano et al., 1997; Morita et al., 1995), there has been increasing interest in incorporating *i*NKT cell activators into strategies for immunotherapy and vaccination (Cerundolo et al., 2009; Kharkwal et al., 2016). The first  $\alpha$ -GalCer developed from systematic structure-activity relationship studies was KRN7000 (Figure 1A) (Kobayashi et al., 1995). In mouse models, KRN7000 also showed potent anti-tumor properties, as well as considerable promise for the treatment of infectious and autoimmune diseases (Cerundolo and Salio, 2007).

Despite the potent immune activating properties of KRN7000, there has been relatively limited success to date in advancing it into clinical use. Small phase 1 trials in human cancer patients have shown, at best, limited evidence of clinical benefit (Nair and Dhodapkar, 2017), and there are features of the response to KRN7000 *in vivo* that may render it suboptimal for tumor immunotherapy and other potential applications (Yu and Porcelli, 2005). A major issue in this regard is the tendency for KRN7000 to elicit high levels of both T helper 1 (Th1) and Th2 associated cytokines, which may have directly conflicting activities leading to ineffective and unpredictable immune responses. This problem has been addressed through the development of structural analogs of KRN7000 that stimulate *i*NKT cell responses that are more biased toward purely Th1 or Th2 cytokine





recognized that identifying ligands that selectively elicit Th1 or Th2 cytokines will likely be crucial for effective therapeutic applications of *i*NKT cell activation (Cerundolo and Salio, 2007; Laurent et al., 2014).

The first Th1-biasing compound reported was  $\alpha$ -C-GalCer (Figure 1A), which showed marked superiority to KRN7000 in mouse cancer and infection models (Kopecky-Bromberg et al., 2009; Schmieg et al., 2003). However, in studies using cell culture models of human *i*NKT cell responses,  $\alpha$ -C-GalCer has been found to be only weakly stimulatory, suggesting that it may not be suitable for development as a human therapeutic (Li et al., 2009a, 2009b; Venkataswamy et al., 2014). Another strongly Th1-biasing *i*NKT cell agonist that was previously identified is the aminodiol (sphinganine) analog (AH03-1 in Figure 1A) of KRN7000, which has activities similar to  $\alpha$ -C-GalCer in mouse models (Arora et al., 2011). AH03-1 and other related sphinganine analogs have generally been found to be highly active *in vivo* in mice or *in vitro* with mouse cells (Brossay et al., 1998; Ndonye et al., 2005; Sidobre et al., 2004), although two previous studies found that they were not efficient activators in cell culture models of human *i*NKT cell responses (Brossay et al., 1998; Dangerfield et al., 2012). Among the more recently reported Th1-biasing analogs of  $\alpha$ -GalCer are those in which the sugar has been modified by C6''-substituted amides, carbamates, and ureas. Some, such as NU- $\alpha$ -GalCer and PyrC- $\alpha$ -GalCer (Figure 1A), show promising anti-tumor activity in mice and elicit a Th1-biased response in studies using human *i*NKT cells *in vitro* (Aspeslagh et al., 2011, 2013).

Considering the responses of selected C6''-substituted compounds in human cell lines and the strongly biased Th1 response elicited by the sphinganine-containing AH03-1, we have explored whether combining a C6'' substitution with a sphinganine variant of  $\alpha$ -GalCer could provide useful synergistic effects. Herein we report studies on a  $\alpha$ -GalCer analog, designated AH10-7, which incorporates a C6'' hydrocinnamoyl ester and lacks the C4'-OH of the sphingoid base. Using a combination of *in vitro* studies and *in vivo* analysis with wild-type and partially humanized mice, we found that the dual modifications in AH10-7 led to preservation of substantial potency in both mouse and human models of *i*NKT cell activation while maintaining the Th1-biasing property of other sphinganine derivatives. Structural studies by X-ray crystallography and *in silico* modeling provided a mechanistic basis for the effect of the C6'' substitution on enhancing presentation of AH10-7 by human CD1d. Our results, along with another recently published study of combining C6'' substitutions with other Th1-biasing modifications (Guillaume et al., 2017), provide a rare example of two separate glycolipid modifications that synergize to create an analog of KRN7000 with potentially useful properties, suggesting a new approach to rational design of *i*NKT cell T cell receptor (TCR) ligands.

## RESULTS

### Synthesis and Bioactivity of an $\alpha$ -GalCer Derivative Combining Sphinganine and C6'' Modifications

To examine the impact of linking an aromatic group to the sugar C6'' in combination with removal of the 4'-OH of the phytosphingosine chain, we synthesized the sphinganine-containing compound AH10-7 and, for comparison, its phytosphingosine

congener AH15-1, as outlined in Figure 1B. Both glycolipids were prepared by the glycosylation of known protected forms **1** (Ndonye et al., 2005) and **2** (Kim et al., 2004) of their respective ceramides (Figure 1B). Thiophenyl-activated carbohydrate **3**, used for both glycosylations, was prepared by esterification of a previously described, partially protected thiophenyl galactose (Bourgeaux and Combret, 2000; Ziegler et al., 1999). The coupling reactions between **3** and **1** or **2** gave high  $\alpha$ -selectivity, and the resultant  $\alpha$ -GalCers were deprotected under standard conditions to give AH10-7 and AH15-1.

Initial assessment of bioactivity was done using cell culture with a mouse *i*NKT cell hybridoma (DN3A4-1.2) and bone marrow-derived dendritic cells (DCs) (Im et al., 2009). To assess presentation of the glycolipids by mouse (m) versus human (h) CD1d, we used bone marrow-derived DCs from either wild-type or human CD1d knock-in (hCD1d-KI) mice. The latter, in which the coding sequence of the mouse *CD1D* gene has been replaced by the orthologous human *CD1D* sequence, has been previously described as a partially humanized mouse model for the study of *i*NKT cell responses (Wen et al., 2013, 2015). Measurement of interleukin (IL)-2 release as an indicator of *i*NKT cell activation showed similar potency over a wide range of concentrations for KRN7000 and both sphinganine derivatives (AH03-1 and AH10-7, Figure 2A) when presented by mCD1d. In contrast, with hCD1d-expressing DCs, AH03-1 showed minimal ability to stimulate the mouse *i*NKT cell hybridoma, whereas AH10-7 retained partial activity relative to KRN7000.

These findings with a canonical *i*NKT cell line expressing a single clonal antigen receptor (TCR) indicated that the addition of the C6'' hydrocinnamoyl group partially restored hCD1d presentation of a sphinganine derivative of KRN7000. To extend this to *i*NKT cells with more heterogeneous TCRs, we sorted *i*NKT cells from the spleens of both wild-type and hCD1d-KI mice and fused these to thymoma line BW5147 $\alpha$ . $\beta$ <sup>-</sup> to generate polyclonal *i*NKT cell lines (Johnson et al., 2017). Similar to the results with the clonal mouse *i*NKT cell line, we found that a polyclonal *i*NKT cell line from wild-type mice showed nearly equivalent responses to the three glycolipids when presented by mCD1d, while a marked reduction in responses was seen for AH03-1 but not AH10-7 when presented by hCD1d (Figure 2B, left). A similar trend, although slightly less pronounced, was observed for a polyclonal *i*NKT cell line derived from hCD1d-KI mice (Figure 2B, right).

We further investigated the differential presentation of AH10-7 and AH03-1 by hCD1d using fully human cell culture systems. Stimulation of human *i*NKT cell clones with the glycolipids in the presence of human monocyte-derived DCs or hCD1d-transfected HeLa cells showed a significant diminution of activity compared with KRN7000 with the sphinganine derivative AH03-1, which was partially reversed by the C6'' substitution in AH10-7 (Figure 2C). In addition, we analyzed proliferation and expansion of primary *i*NKT cells in human peripheral blood mononuclear cell (PBMC) cultures from four normal blood donors, which showed a similarly enhanced activity of AH10-7 compared with the minimal expansion and proliferation induced by AH03-1 (Figure 3). Taken together, these *in vitro* studies indicated that the 4'-OH group of the sphingoid base had an important influence on presentation of  $\alpha$ -GalCer by hCD1d but not mCD1d, and that the defect in presentation of a sphinganine

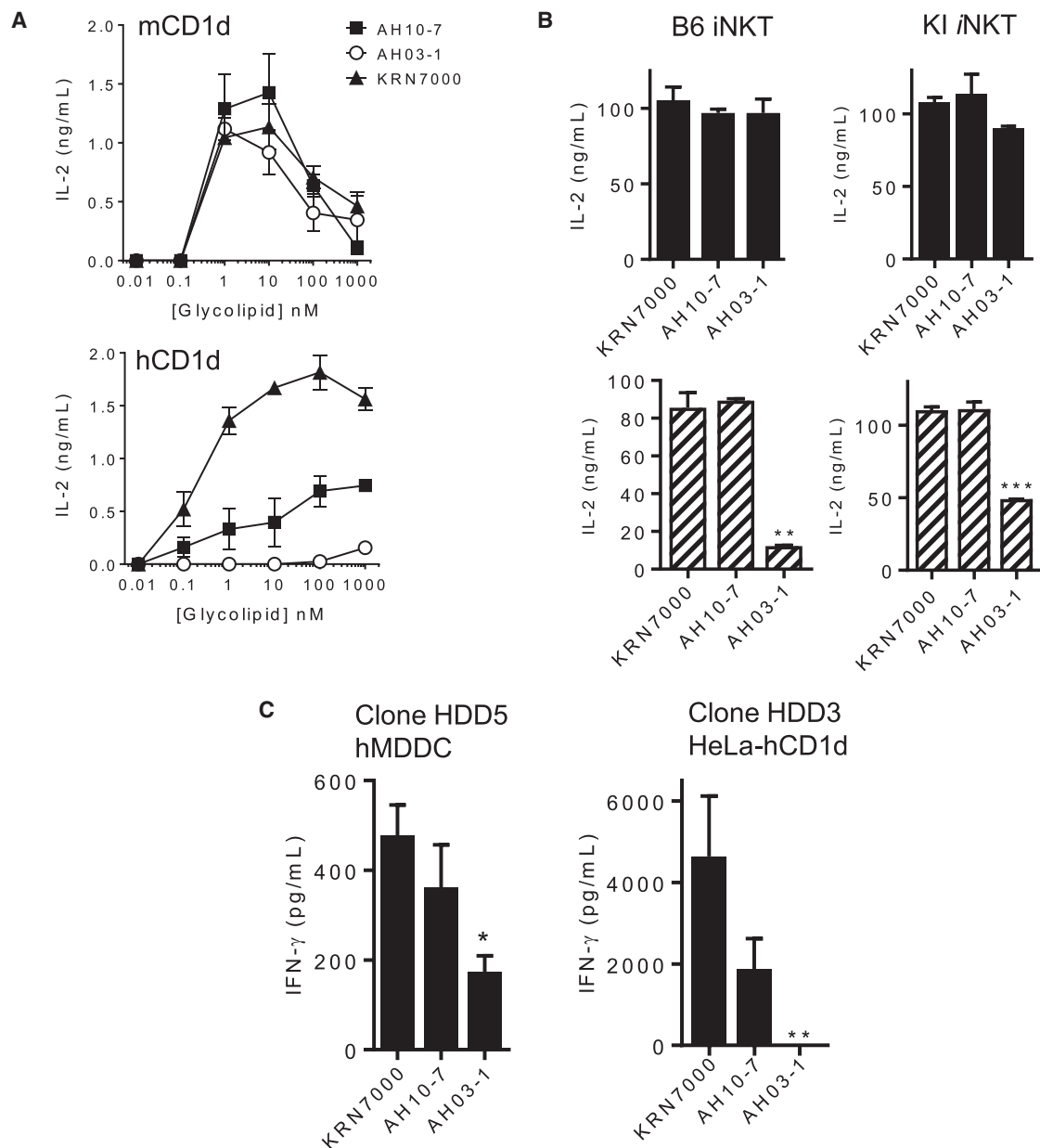


**Figure 2. In Vitro iNKT Cell Activation by 4'-Deoxyphytosphingosine Variants of  $\alpha$ -GalCer**

(A) Activation of mouse iNKT cell hybridoma DNA3.4-1.2 by KRN7000 or 4'-deoxy variants AH03-1 and AH10-7. The indicated concentrations of glycolipids were added to co-cultures of DNA3.4-1.2 cells with bone marrow-derived dendritic cells (BMDCs) from either wild-type C57BL/6 mice (top, mCD1d) or from hCD1d-KI mice (bottom, hCD1d). Activation of iNKT hybridoma cells was determined by measurement of IL-2 levels in culture supernatants by ELISA after 18 hr of culture. Symbols show means and error bars represent  $\pm 1$  SE for triplicate values, and results shown are representative of five separate experiments.

(B) Polyclonal iNKT cell hybridoma lines derived from wild-type C57BL/6 mice (left, B6 iNKT) or from hCD1d KI mice (right, KI iNKT) were co-cultured with either wild-type BMDCs (top, filled bars) or hCD1d-KI BMDCs (bottom, hatched bars) plus 100 nM of the indicated glycolipids. Activation of iNKT hybridoma cells was determined by measurement of IL-2 secretion at 18 hr. Results shown are means  $\pm 1$  SE for duplicate samples, and are representative of two separate experiments.

(C) Left: responses of human iNKT cell clone HDD5 co-cultured with human monocyte-derived dendritic cells (hMDDC) and 100 nM of the indicated glycolipids. Supernatants were harvested after 24 hr of culture for measurement of IFN $\gamma$  levels. Right: responses of human iNKT cell clone HDD3 to 100 nM of the indicated glycolipids presented by HeLa cells transfected with hCD1d. Results shown are means  $\pm 1$  SE for triplicate samples, and are representative of three separate experiments.

Significant differences compared with response to KRN7000 in (B) and (C) are indicated by asterisks: \*,  $p < 0.05$ ; \*\*,  $p < 0.01$ ; \*\*\*,  $p < 0.001$  (ANOVA with Dunnett post-test for multiple comparisons).



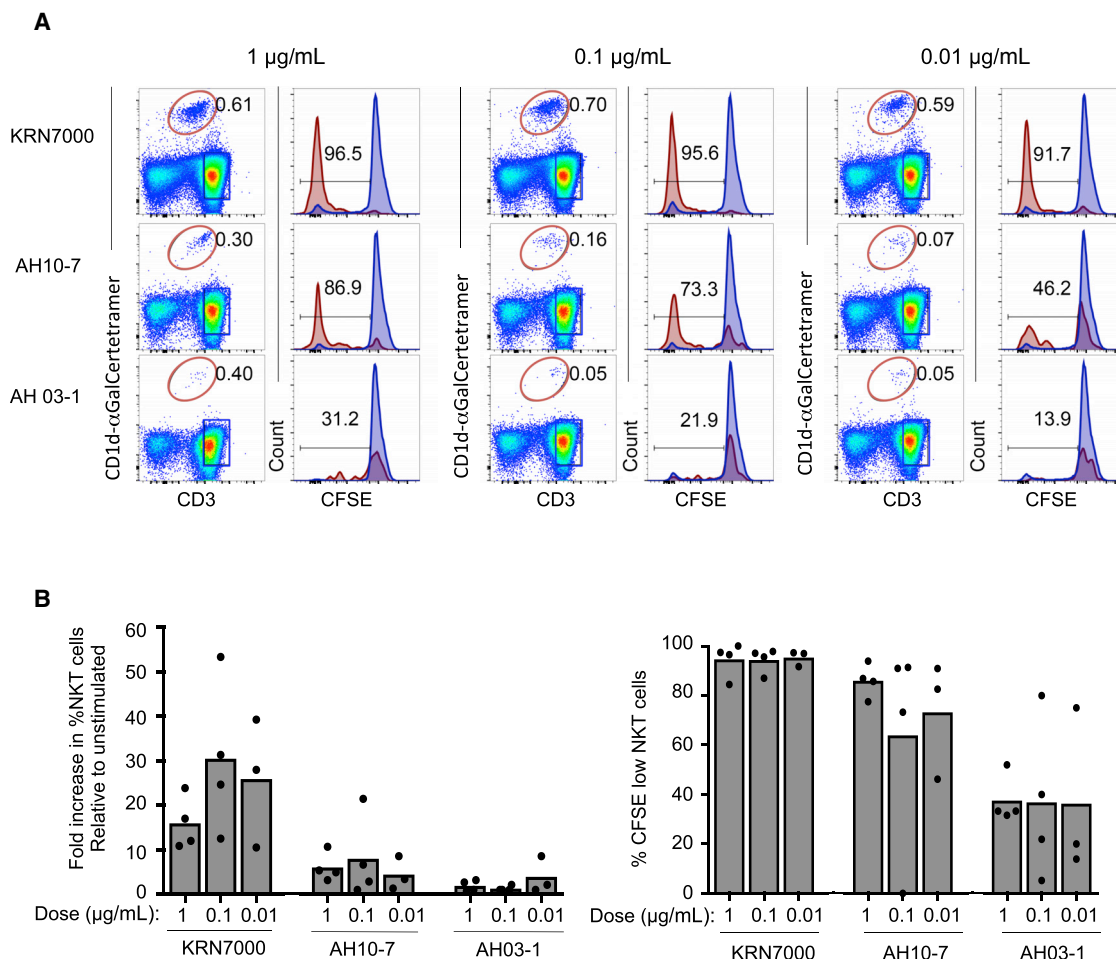


**Figure 3. Expansion and Proliferation of Human Peripheral Blood iNKT Cells**

(A) Carboxyfluorescein succinimidyl ester (CFSE)-labeled human PBMCs were pulsed with respective lipids and cultured for 7 days in the presence of 50 U/mL human IL-2. Representative fluorescence-activated cell sorting (FACS) plots from one donor show  $\alpha$ -GalCer loaded CD1d tetramer-positive iNKT cells (red ovals) and tetramer-negative CD3<sup>+</sup> T cells (blue rectangular regions), followed by the histograms of cells that have proliferated based on CFSE dilution. Blue histograms are tetramer-negative CD3<sup>+</sup> T cells, and red histograms are tetramer-positive iNKT cells.

(B) Graphs depict the fold expansion of iNKT cell percentages at the end of culture relative to the unstimulated sample (left), and the percentage of iNKT cells that have proliferated based on CFSE dilution (right). Each scatter point represents an independent donor sample, and bars show mean values for three or four donors.

derivative by hCD1d could be significantly overcome by incorporation of the C6'' hydrocinnamoyl group in AH10-7.

### Cytokine Biasing Properties and *In Vivo* Activity of AH10-7

Previous studies have attributed a strong Th1-type cytokine bias to the sphinganine derivative AH03-1 in mice and correlated this with its presentation by CD1d proteins that localized preferentially to lipid raft microdomains in the plasma membrane of antigen-presenting cells (Arora et al., 2011, 2016). We tested whether AH10-7 preserved the lipid raft localization by measuring the detergent sensitivity to elution of  $\alpha$ -GalCer-mCD1d complexes from the surface of dendritic cells using a previously described flow cytometry-based assay (Arora et al., 2011) (Figure 4A). As previously shown, complexes of CD1d with the Th1-biasing sphinganine derivative AH03-1 showed greater resistance to detergent elution from the plasma

membrane compared with KRN7000, consistent with strong localization to lipid raft microdomains. For comparison, the strongly Th2-biasing glycolipid  $\alpha$ -GalCer C20:2 (Figure 1A) showed rapid and nearly complete elution from the plasma membrane. AH10-7 behaved similarly to AH03-1 in this assay, showing strong lipid raft localization of its presentation. This was attributable to its sphinganine modification, since a phytosphingosine variant of AH10-7 (AH15-1, Figure 1B) behaved no differently than KRN7000 in this assay (Figure 4A).

The preferential lipid raft localization of CD1d- $\alpha$ -GalCer complexes formed with AH10-7 suggested that this compound was likely to stimulate a Th1 cytokine bias *in vivo*, such as that previously shown for  $\alpha$ -C-GalCer and AH03-1 in mice (Arora et al., 2011; Im et al., 2009; Schmiege et al., 2003). Measurement of serum levels of IFN $\gamma$  and IL-4 after glycolipid injection into mice showed a significant enhancement of IFN $\gamma$  without increases in IL-4 for AH10-7 compared with KRN7000 (Figure 4B).

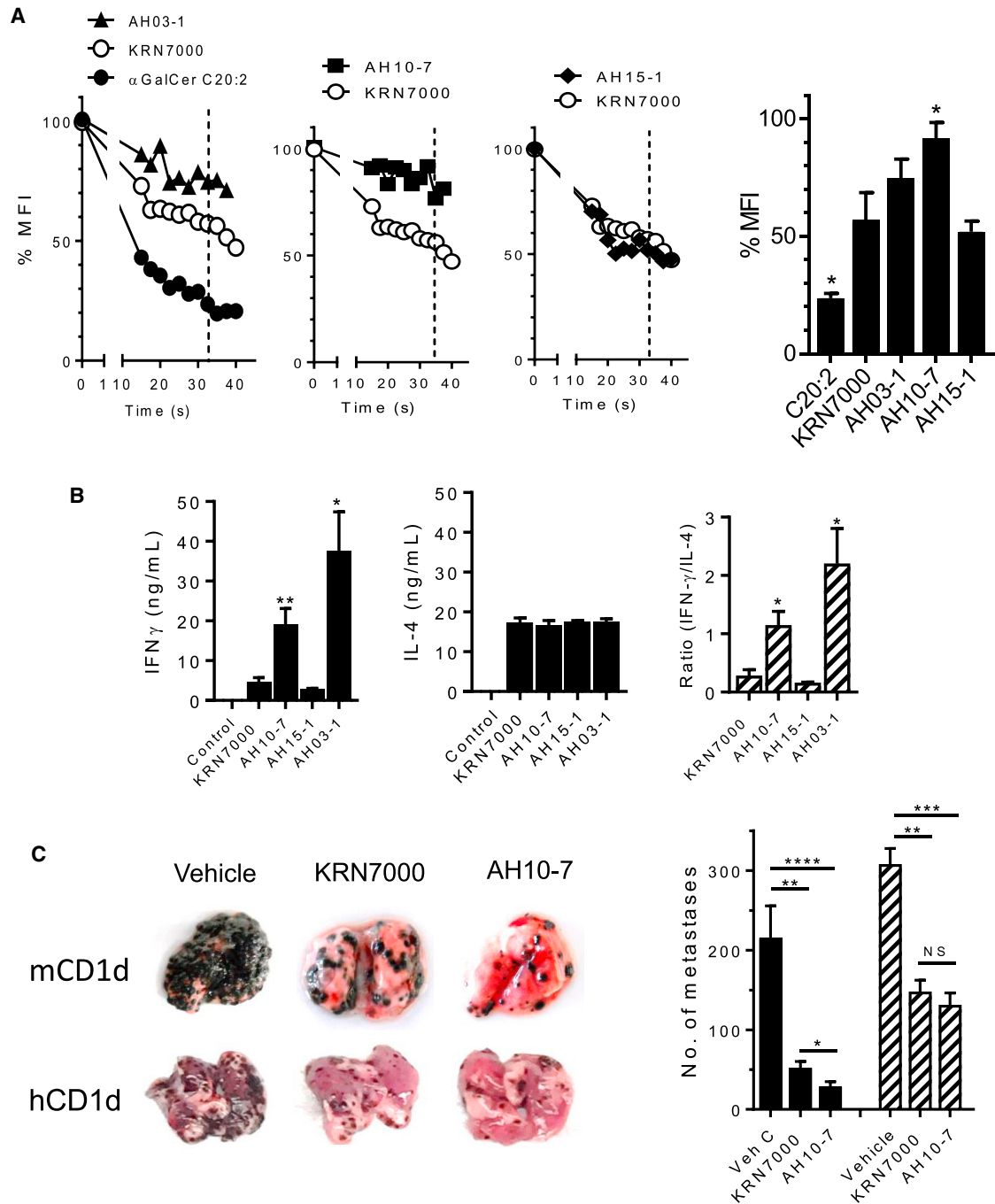


**Figure 4. Cytokine Bias and *In Vivo* Activity of 4'-Deoxyphytosphingosine Variants**

(A) Enhanced plasma membrane lipid raft association of CD1d proteins presenting 4'-deoxyphytosphingosine variant AH10-7. Mouse JAWS II dendritic cells were preincubated with glycolipids to allow loading of CD1d molecules and then labeled by cell surface binding of fluorochrome conjugated mCD1d/ $\alpha$ -GalCer complex-specific mAb L363. Cells were then treated with 0.05% Triton X-100, and elution of cell surface CD1d/glycolipid complexes was monitored over time by flow cytometry. Starting values for mean fluorescence intensity (MFI) were normalized to 100%, and the change in MFI values over time are plotted for cells loaded with KRN7000 and the other indicated glycolipids. Values at 32.5 s post detergent addition (vertical dashed lines) for a minimum of four replicate samples were averaged, and the mean  $\pm$  1 SE for percentage residual MFI is plotted in the bar graph on the right. Results shown are representative of three separate experiments.

(B) Serum cytokine levels following systemic injection of glycolipids. Wild-type C57BL/6 mice were injected intravenously (i.v.) with 4 nmol of each glycolipid or control vehicle (N = 3 mice per group). Serum was collected at 2 and 24 hr post injection. Mean values  $\pm$  1 SE for IFN $\gamma$  levels at 24 hr and IL-4 levels at 2 hr are shown (solid bars), and also the calculated ratios of these cytokines for each glycolipid (hatched bars). Results shown are representative of three separate experiments.

(legend continued on next page)

In contrast, AH15-1, which retains the 4'-OH group in the sphingoid base, produced levels of both cytokines that were similar to those elicited by KRN7000. The altered ratio of IFN $\gamma$  to IL-4 stimulated by AH10-7 was consistent with a Th1-biasing effect for this glycolipid that was significantly augmented compared with KRN7000 or AH15-1, although less pronounced than with AH03-1. Given the association of Th1-biasing properties with improved anti-cancer effects in mice (Schmiege et al., 2003; Venkataswamy and Porcelli, 2010), we tested the impact of AH10-7 compared with KRN7000 in the mouse B16-F10 melanoma model of metastatic cancer (Wen et al., 2013). This revealed strong anti-tumor activity of AH10-7 in both wild-type and hCD1d-KI mice (Figure 4C), which was at least as great as for KRN7000 in this model.

### Structural Analysis of the CD1d-AH10-7 Complex and Its Molecular Interactions with the iNKT TCR

In order to gain structural insights into the molecular recognition of AH10-7 in comparison with KRN7000, we generated complexes *in vitro* of mCD1d loaded with these glycolipids and co-crystallized them with the 2C12 iNKT TCR (Brennan et al., 2017; Pellicci et al., 2009; Wang et al., 2010). We used X-ray crystallography to determine the three-dimensional structures of these ternary complexes to 3.2 Å resolution for AH10-7 and 2.6 Å for KRN7000 (Figure 5A and Table S1). In both complexes, the electron density at the molecular interface between the mCD1d-glycolipid complexes and the 2C12 iNKT TCR was unambiguous. Most notably, distinct electron density corresponding with the *in vitro* loaded glycolipid antigens emerged from within the A'- and F'-portals of mCD1d and protruded out from the antigen-binding cleft (Figures 5A and S1).

The overall docking mode adopted by the 2C12 iNKT TCR to recognize mCD1d presenting KRN7000 and AH10-7 was conserved and was similar to the one previously observed in other crystal structures of iNKT TCR-CD1d- $\alpha$ -GalCer ternary complexes (Girardi et al., 2011; Rossjohn et al., 2012) (Figures 5B and S2). In both complexes, the 2C12 iNKT TCR adopted a parallel docking mode (docking angle of  $\sim 15^\circ$ ) over the F' pocket of mCD1d. Upon 2C12 iNKT TCR ligation, the total buried surface area (BSA) of the TCR at the interface in both ternary complexes was  $\sim 800 \text{ \AA}^2$ . The TCR  $\alpha$  chain contributed the most to the BSA (60% of total), and this was mainly through the complementarity-determining region (CDR) 3 $\alpha$  (44% of BSA). Here, the CDR3 $\alpha$  bridged the  $\alpha 1$ - and  $\alpha 2$ -helices of mCD1d, with Asp94 $\alpha$  and Arg95 $\alpha$  hydrogen bonded to Arg79 and Asp80 (Figure 5B, left). The contribution of the TCR  $\beta$  chain to the binding interface was more limited and was evenly shared, mainly by the CDR2 $\beta$ , CDR3 $\beta$ , and two framework residues (Tyr48 $\beta$  and Glu56 $\beta$ ) (Figure 5B, right), each accounting for a 10%–15% BSA (Figure S2).

The distinct electron density not accounted for by polypeptide residues in the mCD1d-binding groove enabled us to model

unambiguously AH10-7 and KRN7000 in both ternary complexes (Figures 5C and S1). For both glycolipids, the hydrophobic N-acyl and sphingoid base chains were positioned deep within the A' and F' pockets of mCD1d, respectively, whereas the galactose polar moiety largely protruded out of the binding groove to interact with the TCR. Although the sphinganine of AH10-7 and phytosphingosine of KRN7000 adopted similar positions within the F' pockets, we noted that the 4'-OH in the phytosphingosine chain enabled an additional hydrogen bond to Asp80 of mCD1d (Figure 5B). The static crystal structures did not detect rearrangement of the overall positioning of the glycolipid or significant impact on the mCD1d protein structure as a result of the presence or absence of this additional bond. However, as indicated by modeling studies (see below), the impact of removing the 4'-OH may be greater in hCD1d, potentially contributing to the apparent reduction in human iNKT cell responses promoted by AH03-1.

The interactions of the 2C12 iNKT TCR with KRN7000 and AH10-7 bound in mCD1d were exclusively mediated by the TCR  $\alpha$  chain. In both ternary complexes, the galactose was located in a similar position and interacted exclusively with the CDR1 $\alpha$  and CDR3 $\alpha$  loops, with the C2'' and C3'' hydroxyl groups of the sugar forming hydrogen bonds with residues Arg95 $\alpha$  and Asn30 $\alpha$ , respectively (Figure 5C). It was noteworthy that the hydrocinnamoyl ester moiety of AH10-7 was positioned over the A' pocket of mCD1d between Met69 and Met162 and interacted with Thr159 via van der Waals contacts. This pointed to a role for the C6'' substitution in strengthening the binding of AH10-7 to mCD1d and stabilizing the position of the galactosyl head group for TCR recognition.

To directly assess the binding affinity of the iNKT cell TCR to the mCD1d protein loaded with AH10-7 versus KRN7000, we analyzed binding by surface plasmon resonance using the same soluble NKT TCR and mCD1d proteins used to generate the crystal structures of the ternary complexes (Figure 6A). Similar binding affinities of the TCR were observed for both AH10-7 and KRN7000 loaded mCD1d complexes ( $K_d \sim 100\text{--}110 \text{ nM}$ ), which was consistent with the close superposition of the galactose ring and other components of the TCR docking site in the crystal structures (Figure 6B). Comparison of AH10-7 with other C6''-substituted  $\alpha$ -GalCer derivatives previously reported to show high levels of iNKT cell stimulatory activity indicated that all of these preserved a similar positioning of the galactose ring (Aspesslagh et al., 2013 and Figure 6C), underscoring the importance of this feature in maintaining TCR binding affinity.

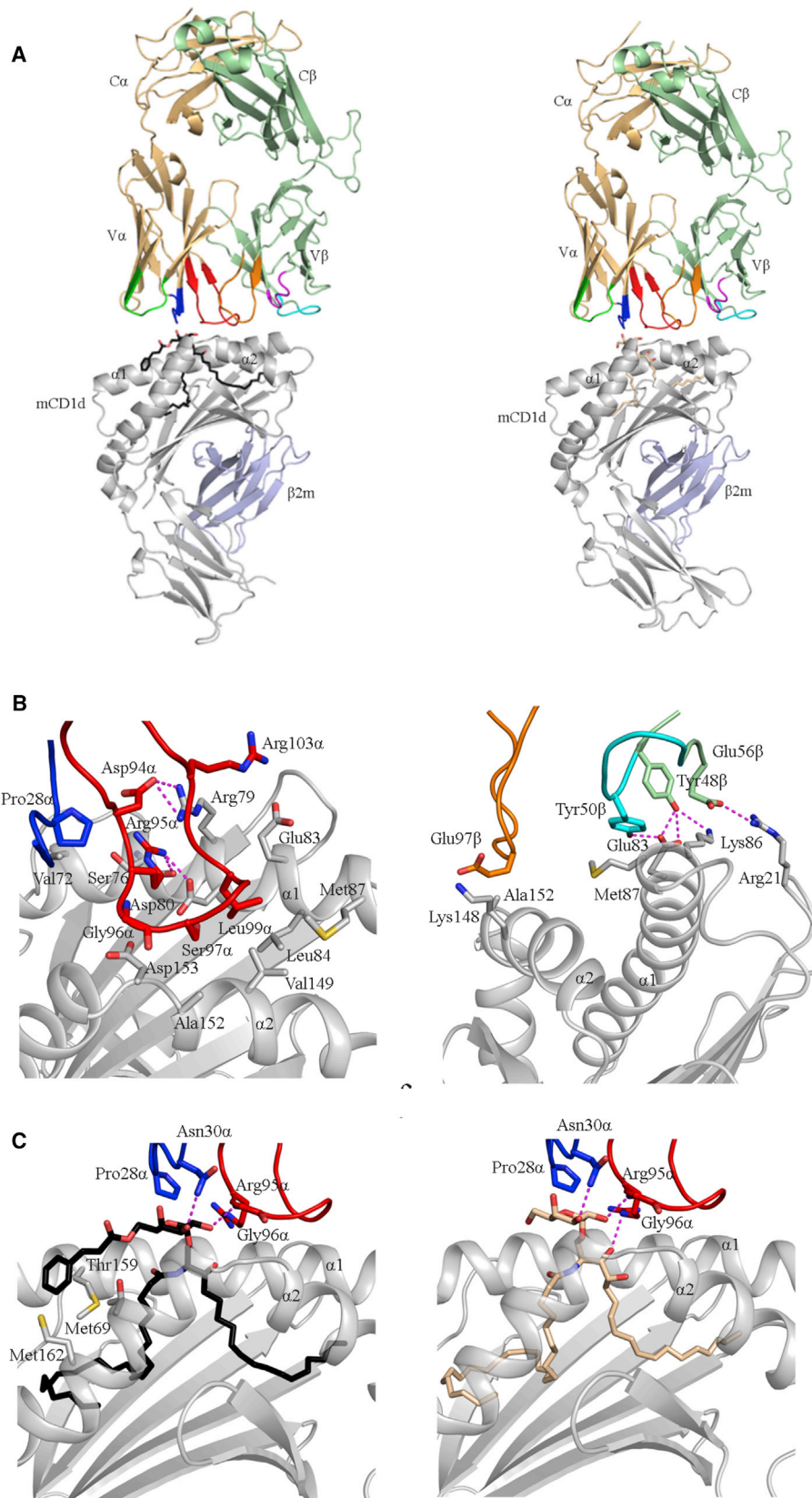
### In Silico Modeling and Computational Analysis of AH10-7 Interactions

The crystal structure of the 2C12 TCR-mCD1d-AH10-7 ternary complex provided an opportunity to use molecular modeling to

(C) *In vivo* antitumor activity of glycolipid AH10-7. Wild-type C57BL/6 or hCD1d-KI mice were injected i.v. with  $3 \times 10^5$  B16-F10 melanoma cells. Two days later, groups of 11–15 mice received i.v. injections of KRN7000, AH10-7 (4 nmol), or vehicle. Animals were sacrificed 15 days later, lungs were removed, and the numbers of tumor nodules were counted visually. Images on the left are representative lungs from wild-type C57BL/6 or hCD1d-KI from each of the treatment groups. Graphs on the right show mean values  $\pm 1$  SE for mice treated with vehicle or glycolipids in the wild-type mice (filled bars) or hCD1d-KI mice (hatched bars). This experiment was carried out twice in wild-type mice, and once in hCD1d-KI mice.

Asterisks indicate significant differences compared with KRN7000 for (A) and (B), or for the indicated comparisons in (C). \*,  $p < 0.05$ ; \*\*,  $p < 0.01$ ; \*\*\*,  $p < 0.001$ ; and \*\*\*\*,  $p < 0.0001$  (ANOVA with Dunnet post-test for multiple comparisons).





(legend on next page)

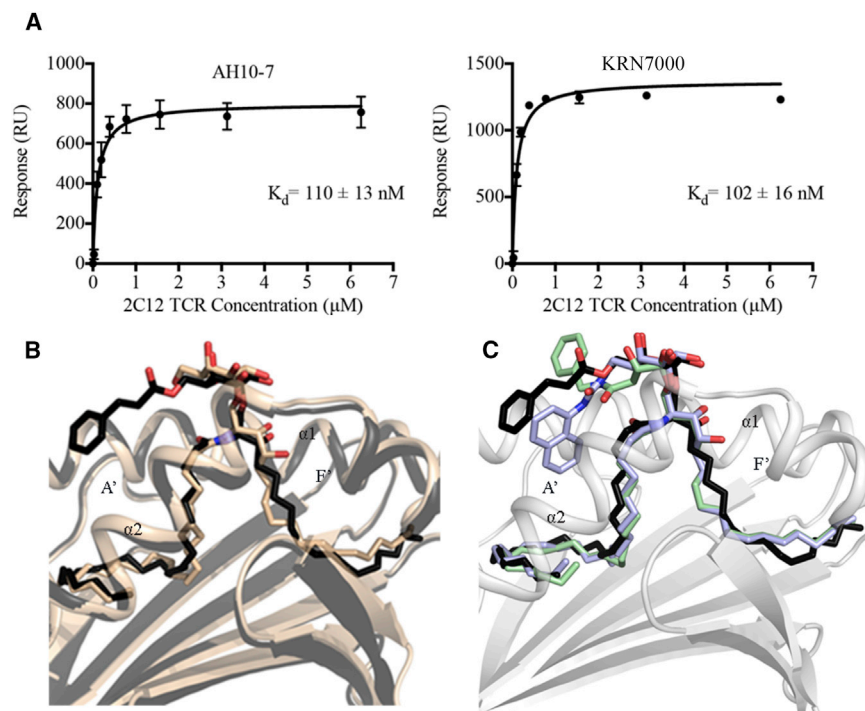


**Figure 6. Affinity and Structural Basis for iNKT Cell TCR Binding to C6'-Modified Variants of KRN7000**

(A) Affinity measurements of the 2C12  $\alpha\beta$  TCR against mCD1d-AH10-7 and mCD1d-KRN7000. The relative binding affinities for each TCR were measured by surface plasmon resonance. Error bars show SEM of two replicates ( $n = 2$ ). RU, response units.

(B) Superposition of the CD1d/glycolipid complexes from the 2C12 TCR-mCD1d-AH10-7 and 2C12 TCR-mCD1d-KRN7000 ternary structures. The superposition of both structures is based on the C $\alpha$  alignment of the mCD1d. In the 2C12 TCR-mCD1d-AH10-7 complex, mCD1d (cartoon) and AH10-7 (sticks) are colored in black, while the 2C12 TCR-mCD1d-KRN7000, mCD1d, and KRN7000 are colored in wheat.

(C) Superposition of the 2C12 TCR-mCD1d-AH10-7, 2C12 TCR-mCD1d-BnNH-GSL, and 2C12 TCR-mCD1d-NU- $\alpha$ -GalCer. For clarity, only mCD1d (light gray) from the 2C12 TCR-mCD1d-AH10-7 ternary complex is shown. The lipid-antigens AH10-7, BnNH-GSL-1', and NU- $\alpha$ -GalCer are colored in black, pale green, and light blue, respectively.

further explore how the sphingoid base and sugar modifications synergize to generate the observed effects of AH10-7 on iNKT cell activation. We used grid-based ligand docking simulations to examine the interactions of similar ligands with and without the 4'-OH (KRN7000 and AH03-1) and the C6'' modification (AH15-1 and AH10-7). As a validation of this approach, we showed that the simulated binding pose of AH10-7 reproduced well the 2C12 TCR-mCD1d-AH10-7 ternary complex structure obtained by X-ray crystallography (Figure 7A). Docking also predicted that this ligand and its phytosphingosine congener AH15-1 adopt a similar binding mode in complexes with hCD1d and the iNKT TCR (Figure S3). As in the experimentally determined structure (Figure 5), the most favored docking poses modeled for AH10-7 in the ternary mouse complex showed that Lys65, His68, and Met162 formed the sides, and Met69 the floor of a cleft on mouse CD1d above the A' pocket to accommodate the hydrocinnamoyl substituent (Figure 7A). This cleft provides a hydrophobic shelter for the hydrocinnamoyl group that enables  $\pi$ -cation and  $\pi$ - $\pi$  interactions with the side chain ammonium of mCD1d-Lys65 and imidazole of mCD1d-His68. By contrast, the favored poses of AH10-7 and AH15-1 modeled in the human ternary complex interdigitated the phenyl of the hydrocinnamoyl group between hCD1d-His68 and hCD1d-Trp153 to potentially realize  $\pi$ - $\pi$  stacking interactions with both of these residues (Figures 7B and S3).

The *in silico* docking procedure provided structures from which binding energies could be calculated using a hybrid quantum mechanics/molecular mechanics (QM/MM) protocol (Duff et al., 2011). The computed binding energies (Figure 7E) correlated with experimental bioactivity trends (Figures 2 and 3). Consistent with the observed trends in biological potencies, AH03-1 was found to have a less favorable binding energy relative to KRN7000 in the human versus mouse ternary complex (Figure 7E). Specifically, the sphingoid base in AH03-1 undergoes a displacement due to the absence of the 4'-OH that results in a net reduction of stabilizing van der Waals contacts with Tyr73 from CD1d. In contrast, the glycolipids with carbohydrate modifications (AH10-7 and AH15-1) were predicted to have more favorable binding in either the human or mouse system, suggesting that functionally relevant contacts realized through carbohydrate modification compensated for the lost interactions of the sphingoid base 4'-OH. In this manner, specific interactions established by the C6''-hydrocinnamoyl moiety improved binding energetics and correlated with the increased potency of AH10-7 for hCD1d presentation.

## DISCUSSION

Sphinganine derivatives were identified by us and others in previous studies as attractive alternatives to phytosphingosine-containing  $\alpha$ -glycosylceramides as iNKT cell activators

**Figure 5. Crystal Structures of TCR-mCD1d-Glycolipid Ternary Complexes**

(A) Cartoon representations of the 2C12  $\alpha\beta$  TCR-mCD1d-AH10-7 (left) and 2C12  $\alpha\beta$  TCR-mCD1d-KRN7000 (right) ternary complexes: mouse CD1d, gray;  $\beta$ 2m, light blue; TCR  $\alpha$ -chain framework, light orange; TCR  $\beta$ -chain framework, pale green; CDR1 $\alpha$ , blue; CDR2 $\alpha$ , green; CDR3 $\alpha$ , red; CDR1 $\beta$ , magenta; CDR2 $\beta$ , cyan; CDR3 $\beta$ , orange; AH10-7, black sticks; KRN7000, pale yellow sticks.

(B) Molecular interactions of the 2C12 TCR  $\alpha$  and  $\beta$  chains with mCD1d. The CDR loops are colored as in (A), and the  $\beta$ -chain framework residues are colored in pale green (structures shown are from the 2C12  $\alpha\beta$  TCR-mCD1d-AH10-7 complex and are essentially identical in the KRN7000-containing complex).

(C) Molecular interactions of the 2C12  $\alpha\beta$  TCR with the AH10-7 and KRN7000 glycolipid antigens. The AH10-7 and KRN7000 ligands are shown as sticks and colored in black and pale yellow, respectively. Hydrogen bond interactions are shown as magenta dashed lines (see also Figures S1 and S2).

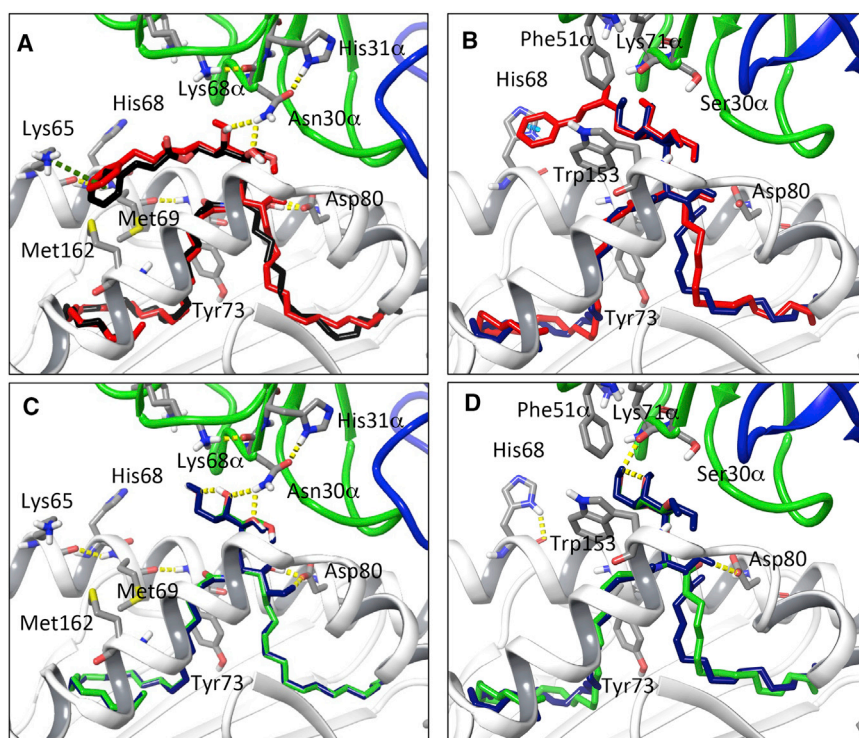


**Figure 7. In Silico Modeling of mCD1d and hCD1d Glycolipid Complexes in Association with iNKT Cell TCR**

(A–D) QM/MM structures of AH10-7 (red), AH03-1 (green), and KRN7000 (blue). The crystallographic pose of AH10-7 is also shown in black in (A). H-bonding, ion- $\pi$  stacking, and  $\pi$ - $\pi$  interactions are indicated by yellow, green, and cyan dashed lines, respectively. (A) and (C) correspond with the mCD1d-TCR complexes, while (B) and (D) correspond with hCD1d-TCR complexes.

(E) QM/MM binding energies for KRN7000, AH15-1, AH03-1, AH10-7 (see also Figure S3).

**E**

	QM/MM Binding Energy (kcal/mol)	
	mCD1d-TCR <sup>b</sup>	hCD1d-TCR <sup>a</sup>
KRN7000	0.0	0.0
AH15-1	-7.6	-6.4
AH03-1	1.2	3.8
AH10-7	-0.2	-0.8

<sup>a</sup>PDB 6BNL; <sup>b</sup>PDB 3VWK

(Lacone et al., 2009; Ndonge et al., 2005). Significantly, sphinganine derivative AH03-1 is one of relatively few analogs known to induce a strongly Th1-biased cytokine response in mice (Arora et al., 2011), a property that correlates with improved anti-cancer and adjuvant effects (Arora et al., 2016; Schmieg et al., 2003). However, at least two previous studies indicated that sphinganine derivatives of KRN7000 may be relatively ineffective in models of human iNKT cell activation (Brossay et al., 1998; Dangerfield et al., 2012), questioning their suitability for further development as therapeutic agents. Given several reports showing enhancement of iNKT cell activation and anti-tumor activity in mice by addition of aromatic ring-containing groups to the C6'' position of the galactose of KRN7000 (Aspeslagh et al., 2011, 2013), we undertook the current study to examine the impact of a relevant C6'' substitution on improving hCD1d presentation of the sphinganine variant (AH03-1) of KRN7000. Our results using several *in vitro* models showed that the compound, AH10-7, which combined a sphinganine base with a C6''-hydrocinnamoyl moiety, had the anticipated effect of enhancing iNKT cell activation when presented by hCD1d. In addition, we found that AH10-7 retained the strong bias toward presentation by CD1d molecules localized to plasma membrane lipid rafts. This is a feature

consistently found for glycolipids that require cellular uptake for intracellular loading onto CD1d (Im et al., 2009), and it correlates strongly with the tendency to induce a proinflammatory Th1 cytokine bias (Arora et al., 2011, 2016). Indeed, we found that AH10-7 induced a significant increase in the systemic levels of IFN $\gamma$  compared with IL-4 after injection into mice, consistent with preservation of lipid raft-dependent presentation of this compound *in vivo*.

Our analysis also took advantage of a hCD1d KI mouse model that more faithfully replicates many of the features of human iNKT cell responses in comparison with standard wild-type mice (Venkataswamy et al., 2014; Wen et al., 2013, 2015). This mouse strain was generated by replacing the mouse genomic segment containing the exons encoding mCD1d with the homologous

human genomic sequence (Wen et al., 2013). Expression of hCD1d in tissues of these mice is similar to its physiologically normal pattern, and they develop a population of endogenous iNKT cells that closely mirrors the numbers, phenotype, and functions of these cells in humans. The use of iNKT cell hybridomas and primary bone marrow-derived DCs from these mice allowed us to acquire further support for the importance of the 4'-OH for effective responses to  $\alpha$ -GalCer in the context of hCD1d presentation. Most notably, AH10-7 was at least as active as KRN7000 for inducing anti-tumor responses against experimental metastases of the B16-F10 melanoma line in both wild-type and hCD1d-KI mice, suggesting that the pairing of structural modifications used in the design of this compound may be a promising path for development of human therapeutics.

A variety of structural and modeling analyses were employed to better understand the molecular basis for the effects of the two modifications to the  $\alpha$ -GalCer structure. These studies revealed that, similar to the previously described structure of other C6''-substituted forms of  $\alpha$ -GalCer bound to CD1d (Aspeslagh et al., 2011, 2013), the aromatic group and its linker to the galactose formed contacts that held it close to the surface of CD1d. This most likely stabilized the position of the galactose of the



bound AH10-7, which was oriented almost identically to the analogous structure with KRN7000 (Figures 6B and S1). The complexes of mCD1d with either of these glycolipids bound had almost identical affinities for at least one mouse *i*NKT cell TCR, as shown using a soluble form of the TCR in surface plasmon resonance studies (Figure 6A). This is consistent with the similar potency of KRN7000 and AH10-7 for activation of *i*NKT T cells with presentation by mCD1d, as observed experimentally (Figure 2).

A plausible explanation for the importance of the 4'-OH group for human but not mouse CD1d presentation was provided by our modeling studies. These strongly suggested that the 4'-OH group is involved in stabilizing or adjusting the conformation of human but not mouse CD1d after binding KRN7000. Interestingly, a marked difference in the sensitivity of human versus mouse CD1d presentation was also noted in previous studies of a truncated phytosphingosine variant of KRN7000 (Im et al., 2009), and structural analyses indicated that this was due to the human protein being intrinsically more sensitive to variations in the lipid chain occupying its F' pocket (McCarthy et al., 2007). Based on our structural studies and modeling analysis, we propose that AH10-7 overcomes this inherent sensitivity of hCD1d to the sphingoid base structure and maintains the correct orientation of the galactose for TCR recognition through interactions of the 6''-hydrocinnamoyl group with the surface of hCD1d. As indicated by our molecular modeling and docking analyses, the interactions of the C6''-hydrocinnamoyl moiety could account for the improved binding energetics predicted by docking (Figure 7E) and potentially explain the increased potency of AH10-7 despite the interactions lost from the absence of the sphingoid base 4'-OH. Given these structural insights, substitution of the phenyl terminus of the C6''-hydrocinnamoyl substituent with electron-withdrawing groups may be a promising direction for future syntheses, since this should favor  $\pi$ - $\pi$  stacking with the electron-rich His68 residue of hCD1d. Further studies along these lines should confirm the usefulness of our docking-QM/MM methodology as an adjunct to other established methods for determining the structure-activity relationship of CD1d-presented ligands and facilitate the development of effective *i*NKT cell activators for translation to clinical applications.

## SIGNIFICANCE

**The CD1d-mediated activation of *i*NKT cells by glycolipids has garnered significant interest because of potential applications in immunotherapy and vaccinations. A problem with the most studied glycolipid ligand and drug, KRN7000, is that it stimulates high levels of both proinflammatory (Th1) and anti-inflammatory (Th2) cytokines, which have conflicting activities that hamper its therapeutic effectiveness. While variants of KRN7000 have been synthesized that elicit a Th1-biased response in mice, these outcomes have not translated well to systems that model human *i*NKT cell responses. For example, one of the most strongly Th1-biasing glycolipids, the sphinganine analog AH03-1, only weakly stimulates human *i*NKT cells. We have demonstrated that incorporating an additional substituent on C6'' of the sugar provides a compound (AH10-7) that recovers**

**much of the activity in models of human *i*NKT cell responses while maintaining Th1-biased stimulation. Indeed, AH10-7 was at least as effective as KRN7000 at suppressing growth of transplantable B16-F10 melanoma in partially humanized mice. A combination of structural, functional, and *in silico* modeling studies indicated that the hydrocinnamoyl moiety on the sugar stabilized the interaction of AH10-7 with CD1d, while the sphinganine modification increased the localization of presentation to lipid raft microdomains of antigen-presenting cells to drive the Th1 bias. These results provide a rare example of synergistic effects attributable to two chemical modifications of a single  $\alpha$ -GalCer compound and have implications for potential applications of sphinganine-containing glycolipids as immunomodulatory drugs or adjuvants.**

## STAR★METHODS

Detailed methods are provided in the online version of this paper and include the following:

- KEY RESOURCES TABLE
- CONTACT FOR REAGENT AND RESOURCE SHARING
- EXPERIMENTAL MODEL AND SUBJECT DETAILS
  - Animals
  - Human Subjects
  - Cell Lines and Primary Cell Cultures
- METHOD DETAILS
  - Glycolipid Synthesis
  - Synthesis and Characterization of AH10-7 and AH15-1
  - Phenyl 2,3,4-Tri-O-benzyl-6-hydrocinnamoyl-1-thio- $\beta$ -D-galactopyranoside (3)
  - Scheme 1. Synthesis of AH10-7
  - (2S,3R)-3-O-Benzyl-1-O-(2,3,4-tri-O-benzyl-6-hydrocinnamoyl- $\alpha$ -D-galactopyranosyl)-2-(N-hexacosanoylamino)octadecan-1,3-diol (A)
  - (2S,3R)-1-O-(6-Hydrocinnamoyl- $\alpha$ -D-galactopyranosyl)-2-(N-hexacosanoylamino)octadecane-1,3-diol (AH10-7)
  - Scheme 2. Synthesis of AH15-1
  - (2S,3S,4R)-3,4-di-O-*tert*-butyldimethylsilyl-1-O-(2,3,4-tri-O-benzyl-6-hydrocinnamoyl- $\alpha$ -D-galactopyranosyl)-2-(N-hexacosanoylamino)octadecan-1,3,4-triol (B)
  - (2S,3S,4R)-1-O-(2,3,4-Tri-O-benzyl-6-hydrocinnamoyl- $\alpha$ -D-galactopyranosyl)-2-(N-hexacosanoylamino)octadecan-1,3,4-triol (C)
  - (2S,3S,4R)-1-O-(6-Hydrocinnamoyl- $\alpha$ -D-galactopyranosyl)-2-(N-hexacosanoylamino)octadecan-3,4-diol (AH15-1)
  - Reconstitution of Glycolipids for *In Vitro* and *In Vivo* Administration
  - CD1d Tetramer Preparation
  - *In Vitro* and *In Vivo* Activation of *i*NKT Cells
  - Lipid Raft Localization of CD1d/Glycolipid Complexes
  - Determination of B16-F10 Melanoma Lung Metastases
  - Expression and Purification of Mouse CD1d and 2C12  $\alpha\beta$  TCR Proteins

- Glycolipid Loading of mCD1d and Purification of Ternary Complexes
- Surface Plasmon Resonance
- X-ray Crystallography
- Computational Methods
- QUANTIFICATION AND STATISTICAL ANALYSIS
- DATA AND SOFTWARE AVAILABILITY

## SUPPLEMENTAL INFORMATION

Supplemental Information includes three figures, three tables, and one data file and can be found with this article online at <https://doi.org/10.1016/j.chembiol.2018.02.009>.

## ACKNOWLEDGMENTS

This work was supported by NIH grants U01 GM111849 (A.R.H., S.A.P., J.A.G., and W.Y.), R01 GM087136 (A.R.H.), R01 AI45889 (S.A.P.), and R01 AI 091987 (W.Y.). M.G.-P. is supported by NSF Fellowship DGE-1247393. L.J.C. is supported by FONDECYT grant 1160336. J.L.N. is supported by an Australian Research Council (ARC) Future fellowship (FT160100074). Flow cytometry resources were supported in part by NCI grant CA13330 (Albert Einstein College of Medicine Cancer Center). This work was also supported by a program grant from the Cancer Council Victoria APP1042866, National Health and Medical Research Council of Australia (NHMRC) (1013667), the Australian Research Council (ARC) (CE140100011 and LP140100920), and the Worldwide Cancer Research (16-1106). D.I.G. was supported by NHMRC Senior Principal Research Fellowships (1020770, 1117766).

## AUTHOR CONTRIBUTIONS

D.C., S.K., and S.K.R. synthesized glycolipids for this study. N.A.S.-A., L.J.C., P.A., J.H.L., X.W., H.-F.K., and W.Y. performed experiments on iNKT cell responses. M.J.G.-P. and J.A.G. did molecular modeling and docking studies. J.L.N., T.Y., S.S., and J.R. did X-ray crystallography, Biacore experiments, and analysis of protein structures. D.I.G., W.Y., J.R., J.L.N., S.A.P., and A.R.H. interpreted results and designed experiments. All authors contributed to writing the manuscript.

## DECLARATION OF INTERESTS

S.A.P. is a paid consultant for Vaccinex (Rochester, N.Y.), which has a proprietary interest in the development of therapeutics based on iNKT cell activators. S.A.P. is named as an inventor on patents related to the use of iNKT cell activators as adjuvants and immunotherapeutic agents (US7063844; US8022043; US9139809; and US9371352). D.I.G. is the chair of the scientific advisory board for Avalia Immunotherapies, a biotech company that deals with  $\alpha$ -GalCer-based vaccines.

Received: November 18, 2017

Revised: January 11, 2018

Accepted: February 16, 2018

Published: March 22, 2018

## REFERENCES

- Arora, P., Baena, A., Yu, K.O., Saini, N.K., Kharkwal, S.S., Goldberg, M.F., Kunnath-Velayudhan, S., Carreno, L.J., Venkataswamy, M.M., Kim, J., et al. (2014). A single subset of dendritic cells controls the cytokine bias of natural killer T cell responses to diverse glycolipid antigens. *Immunity* **40**, 105–116.
- Arora, P., Kharkwal, S.S., Ng, T.W., Kunnath-Velayudhan, S., Saini, N.K., Johndrow, C.T., Chang, Y.T., Besra, G.S., and Porcelli, S.A. (2016). Endocytic pH regulates cell surface localization of glycolipid antigen loaded CD1d complexes. *Chem. Phys. Lipids* **194**, 49–57.
- Arora, P., Venkataswamy, M.M., Baena, A., Bricard, G., Li, Q., Veerapen, N., Ndonge, R., Park, J.J., Lee, J.H., Seo, K.C., et al. (2011). A rapid fluorescence-based assay for classification of iNKT cell activating glycolipids. *J. Am. Chem. Soc.* **133**, 5198–5201.
- Aspeshlagh, S., Li, Y., Yu, E.D., Pauwels, N., Trappeniers, M., Girardi, E., Decruy, T., Van Beneden, K., Venken, K., Drennan, M., et al. (2011). Galactose-modified iNKT cell agonists stabilized by an induced fit of CD1d prevent tumour metastasis. *EMBO J.* **30**, 2294–2305.
- Aspeshlagh, S., Nemčović, M., Pauwels, N., Venken, K., Wang, J., Calenbergh, S.V., Zajonc, D.M., and Elewaut, D. (2013). Enhanced TCR footprint by a novel glycolipid increases NKT-dependent tumor protection. *J. Immunol.* **191**, 2916–2925.
- Bendelac, A., Savage, P.B., and Teyton, L. (2007). The biology of NKT cells. *Annu. Rev. Immunol.* **25**, 297–336.
- Borg, N.A., Wun, K.S., Kjer-Nielsen, L., Wilce, M.C., Pellicci, D.G., Koh, R., Besra, G.S., Bharadwaj, M., Godfrey, D.I., McCluskey, J., et al. (2007). CD1d-lipid-antigen recognition by the semi-invariant NKT T-cell receptor. *Nature* **448**, 44–49.
- Bourgeois, E., and Combret, J.-C. (2000). General access to asymmetric  $\gamma$ -cyclodextrins for gas chromatographic applications by insertion of a selectively modified sugar unit. *Tetrahedron Asymmetry* **11**, 4189–4205.
- Brennan, P.J., Brigi, M., and Brenner, M.B. (2013). Invariant natural killer T cells: an innate activation scheme linked to diverse effector functions. *Nat. Rev. Immunol.* **13**, 101–117.
- Brennan, P.J., Cheng, T.-Y., Pellicci, D.G., Watts, G.F.M., Veerapen, N., Young, D.C., Rossjohn, J., Besra, G.S., Godfrey, D.I., Brenner, M.B., et al. (2017). Structural determination of lipid antigens captured at the CD1d-T-cell receptor interface. *Proc. Natl. Acad. Sci. USA* **114**, 8348–8353.
- Bricard, G., Cesson, V., Devevre, E., Bouzourene, H., Barbey, C., Rufer, N., Im, J.S., Alves, P.M., Martinet, O., Halkic, N., et al. (2009). Enrichment of human CD4<sup>+</sup> V $\alpha$ 24/V $\beta$ 11 invariant NKT cells in intrahepatic malignant tumors. *J. Immunol.* **182**, 5140–5151.
- Bricard, G., Venkataswamy, M.M., Yu, K.O., Im, J.S., Ndonge, R.M., Howell, A.R., Veerapen, N., Illarionov, P.A., Besra, G.S., Li, Q., et al. (2010). A-galactosylceramide analogs with weak agonist activity for human iNKT cells define new candidate anti-inflammatory agents. *PLoS One* **5**, e14374.
- Bricogne, G., Blanc, E., Brandl, M., Flensburg, C., Keller, P., Paciorek, W., Roversi, P., Sharff, A., Smart, O.S., et al. (2017). BUSTER (Global Phasing).
- Brossay, L., Naidenko, O., Burdin, N., Matsuda, J., Sakai, T., and Kronenberg, M. (1998). Structural requirements for galactosylceramide recognition by CD1-restricted NK T cells. *J. Immunol.* **161**, 5124–5128.
- Cerundolo, V., and Salio, M. (2007). Harnessing NKT cells for therapeutic applications. *Curr. Top. Microbiol. Immunol.* **314**, 325–340.
- Cerundolo, V., Silk, J.D., Masri, S.H., and Salio, M. (2009). Harnessing invariant NKT cells in vaccination strategies. *Nat. Rev. Immunol.* **9**, 28–38.
- Dangerfield, E.M., Cheng, J.M., Knight, D.A., Weinkove, R., Dunbar, P.R., Hermans, I.F., Timmer, M.S., and Stocker, B.L. (2012). Species-specific activity of glycolipid ligands for invariant NKT cells. *Chembiochem* **13**, 1349–1356.
- Duff, M.R., Jr., Fyvie, W.S., Markad, S.D., Frankel, A.E., Kumar, C.V., Gascón, J.A., and Peczu, M.W. (2011). Computational and experimental investigations of mono-septanoside binding by Concanavalin A: correlation of ligand stereochemistry to enthalpies of binding. *Org. Biomol. Chem.* **9**, 154–164.
- Emsley, P., Lohkamp, B., Scott, W.G., and Cowtan, K. (2010). Features and development of Coot. *Acta Crystallogr. D Biol. Crystallogr.* **66**, 486–501.
- Forestier, C., Takaki, T., Molano, A., Im, J.S., Baine, I., Jerud, E.S., Illarionov, P., Ndonge, R., Howell, A.R., Santamaria, P., et al. (2007). Improved outcomes in NOD mice treated with a novel Th2 cytokine-biasing NKT cell activator. *J. Immunol.* **178**, 1415–1425.
- Garboczi, D.N., Ghosh, P., Utz, U., Fan, Q.R., Biddison, W.E., and Wiley, D.C. (1996). Structure of the complex between human T-cell receptor, viral peptide and HLA-A2. *Nature* **384**, 134–141.
- Girardi, E., Yu, E.D., Li, Y., Tarumoto, N., Pei, B., Wang, J., Illarionov, P., Kinjo, Y., Kronenberg, M., and Zajonc, D.M. (2011). Unique interplay between sugar and lipid in determining the antigenic potency of bacterial antigens for NKT cells. *PLoS Biol.* **9**, e1001189.



- Guillaume, J., Seki, T., Decruy, T., Venken, K., Elewaut, D., Tsuji, M., and Van Calenbergh, S. (2017). Synthesis of C6''-modified  $\alpha$ -GalCer analogs as mouse and human iNKT cell agonists. *Org. Biomol. Chem.* **15**, 2217–2225.
- Halgren, T.A., Murphy, R.B., Friesner, R.A., Beard, H.S., Frye, L.L., Pollard, W.T., and Banks, J.L. (2004). Glide: a new approach for rapid, accurate docking and scoring. 2. Enrichment factors in database screening. *J. Med. Chem.* **47**, 1750–1759.
- Im, J.S., Arora, P., Bricard, G., Molano, A., Venkataswamy, M.M., Baine, I., Jerud, E.S., Goldberg, M.F., Baena, A., Yu, K.O., et al. (2009). Kinetics and cellular site of glycolipid loading control the outcome of natural killer T cell activation. *Immunity* **30**, 888–898.
- Johnson, A.J., Kennedy, S.C., Lindestam Arlehamn, C.S., Goldberg, M.F., Saini, N.K., Xu, J., Paul, S., Hegde, S.S., Blanchard, J.S., Chan, J., et al. (2017). Identification of mycobacterial RplJ/L10 and RpsA/S1 proteins as novel targets for CD4+ T cells. *Infect. Immun.* **85**.
- Kawano, T., Cui, J., Koezuka, Y., Taura, I., Kaneko, Y., Motoki, K., Ueno, H., Nakagawa, R., Sato, H., Kondo, E., et al. (1997). CD1d-restricted and TCR-mediated activation of valpha14 NKT cells by glycosylceramides. *Science* **278**, 1626–1629.
- Kharkwal, S.S., Arora, P., and Porcelli, S.A. (2016). Glycolipid activators of invariant NKT cells as vaccine adjuvants. *Immunogenetics* **68**, 597–610.
- Kim, S., Song, S., Lee, T., Jung, S., and Kim, D. (2004). Practical synthesis of KRN7000 from phytosphingosine. *Synthesis*, 847–850.
- Kobayashi, E., Motoki, K., Uchida, T., Fukushima, H., and Koezuka, Y. (1995). KRN7000, a novel immunomodulator, and its antitumor activities. *Oncol. Res.* **7**, 529–534.
- Kopecky-Bromberg, S.A., Fraser, K.A., Pica, N., Carnero, E., Moran, T.M., Franck, R.W., Tsuji, M., and Palese, P. (2009). Alpha-G-galactosylceramide as an adjuvant for a live attenuated influenza virus vaccine. *Vaccine* **27**, 3766–3774.
- Lacone, V., Hunault, J., Pipelier, M., Blot, V., Lecourt, T., Rocher, J., Turcot-Dubois, A.L., Marionneau, S., Douillard, J.Y., Clement, M., et al. (2009). Focus on the controversial activation of human iNKT cells by 4-deoxy analogue of KRN7000. *J. Med. Chem.* **52**, 4960–4963.
- Laurent, X., Bertin, B., Renault, N., Farce, A., Specca, S., Milhomme, O., Millet, R., Desreumaux, P., Henon, E., and Chavatte, P. (2014). Switching invariant natural killer T (iNKT) cell response from anticancerous to anti-inflammatory effect: molecular bases. *J. Med. Chem.* **57**, 5489–5508.
- Li, X., Chen, G., Garcia-Navarro, R., Franck, R.W., and Tsuji, M. (2009a). Identification of C-glycoside analogues that display a potent biological activity against murine and human invariant natural killer T cells. *Immunology* **127**, 216–225.
- Li, X., Shiratsuchi, T., Chen, G., Dellabona, P., Casorati, G., Franck, R.W., and Tsuji, M. (2009b). Invariant TCR rather than CD1d shapes the preferential activities of C-glycoside analogues against human versus murine invariant NKT cells. *J. Immunol.* **183**, 4415–4421.
- McCarthy, C., Shepherd, D., Fleire, S., Stronge, V.S., Koch, M., Illarionov, P.A., Bossi, G., Salio, M., Denkberg, G., Reddington, F., et al. (2007). The length of lipids bound to human CD1d molecules modulates the affinity of NKT cell TCR and the threshold of NKT cell activation. *J. Exp. Med.* **204**, 1131–1144.
- McCoy, A.J. (2007). Solving structures of protein complexes by molecular replacement with Phaser. *Acta Crystallogr. D Biol. Crystallogr.* **63**, 32–41.
- McCoy, A.J., Grosse-Kunstleve, R.W., Adams, P.D., Winn, M.D., Storoni, L.C., and Read, R.J. (2007). Phaser crystallographic software. *J. Appl. Crystallogr.* **40**, 658–674.
- Miyamoto, K., Miyake, S., and Yamamura, T. (2001). A synthetic glycolipid prevents autoimmune encephalomyelitis by inducing TH2 bias of natural killer T cells. *Nature* **413**, 531–534.
- Morita, M., Motoki, K., Akimoto, K., Natori, T., Sakai, T., Sawa, E., Yamaji, K., Koezuka, Y., Kobayashi, E., and Fukushima, H. (1995). Structure-activity relationship of alpha-galactosylceramides against B16-bearing mice. *J. Med. Chem.* **38**, 2176–2187.
- Murphy, R.B., Philipp, D.M., and Friesner, R.A. (2000). A mixed quantum mechanics/molecular mechanics (QM/MM) method for large-scale modeling of chemistry in protein environments. *J. Comput. Chem.* **21**, 14421457.
- Nair, S., and Dhodapkar, M.V. (2017). Natural killer T cells in cancer immunotherapy. *Front. Immunol.* **8**.
- Ndonye, R.M., Izmirian, D.P., Dunn, M.F., Yu, K.O., Porcelli, S.A., Khurana, A., Kronenberg, M., Richardson, S.K., and Howell, A.R. (2005). Synthesis and evaluation of sphinganine analogues of KRN7000 and OCH. *J. Org. Chem.* **70**, 10260–10270.
- Pellicci, D.G., Patel, O., Kjer-Nielsen, L., Pang, S.S., Sullivan, L.C., Kyparissoudis, K., Brooks, A.G., Reid, H.H., Gras, S., Lucet, I.S., et al. (2009). Differential recognition of CD1d-alpha-galactosyl ceramide by the V beta 8.2 and V beta 7 semi-invariant NKT T cell receptors. *Immunity* **31**, 47–59.
- Rosjohn, J., Pellicci, D.G., Patel, O., Gapin, L., and Godfrey, D.I. (2012). Recognition of CD1d-restricted antigens by natural killer T cells. *Nat. Rev. Immunol.* **12**, 845–857.
- Sastry, G.M., Adzhigirey, M., Day, T., Annabhimoju, R., and Sherman, W. (2013). Protein and ligand preparation: parameters, protocols, and influence on virtual screening enrichments. *J. Comput. Aided Mol. Des.* **27**, 221–234.
- Schmiege, J., Yang, G., Franck, R.W., and Tsuji, M. (2003). Superior protection against malaria and melanoma metastases by a C-glycoside analogue of the natural killer T cell ligand [alpha]-galactosylceramide. *J. Exp. Med.* **198**, 1631–1641.
- Sidobre, S., Hammond, K.J., Benazet-Sidobre, L., Maltsev, S.D., Richardson, S.K., Ndonye, R.M., Howell, A.R., Sakai, T., Besra, G.S., Porcelli, S.A., et al. (2004). The T cell antigen receptor expressed by Valpha14i NKT cells has a unique mode of glycosphingolipid antigen recognition. *Proc. Natl. Acad. Sci. USA* **101**, 12254–12259.
- Smart, O.S., Womack, T.O., Flensburg, C., Keller, P., Paciorek, W., Sharff, A., Vornrhein, C., and Bricogne, G. (2012). Exploiting structure similarity in refinement: automated NCS and target-structure restraints in BUSTER. *Acta Crystallogr. D Biol. Crystallogr.* **68**, 368–380.
- Spada, F.M., Borriello, F., Sugita, M., Watts, G.F., Koezuka, Y., and Porcelli, S.A. (2000). Low expression level but potent antigen presenting function of CD1d on monocyte lineage cells. *Eur. J. Immunol.* **30**, 3468–3477.
- Tannor, D.J., Marten, B., Murphy, R., Friesner, R.A., Sitkoff, D., Nicholls, A., Honig, B., Ringnalda, M., and Goddard, W.A., III (1994). Accurate first principles calculation of molecular charge distributions and solvation energies from ab initio quantum mechanics and continuum dielectric theory. *J. Am. Chem. Soc.* **116**, 11875–11882.
- Venkataswamy, M.M., Ng, T.W., Kharkwal, S.S., Carreno, L.J., Johnson, A.J., Kunnath-Velayudhan, S., Liu, Z., Bittman, R., Jervis, P.J., Cox, L.R., et al. (2014). Improving *Mycobacterium bovis* bacillus Calmette-Guerin as a vaccine delivery vector for viral antigens by incorporation of glycolipid activators of NKT cells. *PLoS One* **9**, e108383.
- Venkataswamy, M.M., and Porcelli, S.A. (2010). Lipid and glycolipid antigens of CD1d-restricted natural killer T cells. *Semin. Immunol.* **22**, 68–78.
- Wang, J., Li, Y., Kinjo, Y., Mac, T.T., Gibson, D., Painter, G.F., Kronenberg, M., and Zajonc, D.M. (2010). Lipid binding orientation within CD1d affects recognition of *Borrelia burgorferi* antigens by NKT cells. *Proc. Natl. Acad. Sci. USA* **107**, 1535–1540.
- Wen, X., Kim, S., Xiong, R., Li, M., Lawrence, A., Huang, X., Chen, S.Y., Rao, P., Besra, G.S., Dellabona, P., et al. (2015). A subset of CD8alpha/beta+ invariant NKT cells in a humanized mouse model. *J. Immunol.* **195**, 1459–1469.
- Wen, X., Rao, P., Carreno, L.J., Kim, S., Lawrence, A., Porcelli, S.A., Cresswell, P., and Yuan, W. (2013). Human CD1d knock-in mouse model demonstrates potent antitumor potential of human CD1d-restricted invariant natural killer T cells. *Proc. Natl. Acad. Sci. USA* **110**, 2963–2968.
- Winn, M.D., Ballard, C.C., Cowtan, K.D., Dodson, E.J., Emsley, P., Evans, P.R., Keegan, R.M., Krissinel, E.B., Leslie, A.G., McCoy, A., et al. (2011). Overview of the CCP4 suite and current developments. *Acta Crystallogr. D Biol. Crystallogr.* **67**, 235–242.
- Wun, K.S., Ross, F., Patel, O., Besra, G.S., Porcelli, S.A., Richardson, S.K., Keshipetty, S., Howell, A.R., Godfrey, D.I., and Rosjohn, J. (2012). Human

- and mouse type I natural killer T cell antigen receptors exhibit different fine specificities for CD1d-antigen complex. *J. Biol. Chem.* **287**, 39139–39148.
- Yu, K.O., Im, J.S., Illarionov, P.A., Ndonye, R.M., Howell, A.R., Besra, G.S., and Porcelli, S.A. (2007). Production and characterization of monoclonal antibodies against complexes of the NKT cell ligand alpha-galactosylceramide bound to mouse CD1d. *J. Immunol. Methods* **323**, 11–23.
- Yu, K.O., Im, J.S., Molano, A., Dutronc, Y., Illarionov, P.A., Forestier, C., Fujiwara, N., Arias, I., Miyake, S., Yamamura, T., et al. (2005). Modulation of CD1d-restricted NKT cell responses by using N-acyl variants of alpha-galactosylceramides. *Proc. Natl. Acad. Sci. USA* **102**, 3383–3388.
- Yu, K.O., and Porcelli, S.A. (2005). The diverse functions of CD1d-restricted NKT cells and their potential for immunotherapy. *Immunol. Lett.* **100**, 42–55.
- Ziegler, T., Dettmann, R., Ariffadhillah, and Zettl, U. (1999). Prearranged glycosides. Part 8. Intramolecular  $\alpha$ -galactosylation via succinoyl tethered glycosides. *J. Carbohydr. Chem.* **18**, 1079–1095.

## STAR★METHODS

## KEY RESOURCES TABLE

REAGENT or RESOURCE	SOURCE	IDENTIFIER
<b>Antibodies</b>		
L363, anti-mCD1d/ $\alpha$ GalCer complex	Yu et al., 2007	N/A
Rat anti-mouse IL-2 (ELISA capture), clone JES6-1A12	BD Biosciences	Cat# 554424; RRID: AB_395383
Biotinylated Rat anti-mouse IL-2 (ELISA detection), clone JES6-5H4	BD Biosciences	Cat# 554426; RRID: AB_395384
Anti-human IFN $\gamma$ (ELISA capture), clone 2G1	ThermoFisher Scientific	Cat# M700A; RRID: AB_223578
Biotinylated anti-human IFN $\gamma$ (ELISA detection), clone B133.5	ThermoFisher Scientific	Cat# M701B; RRID: AB_223580
Anti-human CD3, clone UCHT1	BD Horizon	Cat# 563546
<b>Bacterial and Virus Strains</b>		
<i>E. coli</i> BL21 (DE3)	Merck	Cat# 69450
<b>Biological Samples</b>		
Human peripheral blood mononuclear cells	Australian Red Cross Blood Service	Agreement # 13-04VIC-07
<b>Chemicals, Peptides, and Recombinant Proteins</b>		
KRN7000 glycolipid	Avanti, and Dr. G. S. Besra, University of Birmingham, UK	<a href="https://avantilipids.com/product/867000/">https://avantilipids.com/product/867000/</a>
AH10-7 glycolipid	This paper	N/A
AH03-1 glycolipid	Ndonye et al., 2005 Dr. Amy Howell University of Connecticut, CT, USA	N/A
AH15-1 glycolipid	This paper	N/A
DB03-4 glycolipid	Yu et al., 2005 Dr. G. S. Besra, University of Birmingham, UK	N/A
PBS-44 glycolipid	Dr. P. Savage, Brigham Young University, USA	N/A
Insect-XPRESS™ Medium	Lonza	<a href="http://www.lonza.com/products-services/bio-research/cell-culture-products/specialty-media/insect-xpress-protein-free-insect-cell-medium-with-l-glutamine.aspx">http://www.lonza.com/products-services/bio-research/cell-culture-products/specialty-media/insect-xpress-protein-free-insect-cell-medium-with-l-glutamine.aspx</a>
Fetal Calf Serum	Atlanta Biologicals	Cat# S11150
Triton X-100	Sigma	Cat# T8787
Tween-20	ThermoFisher	Cat# BP337-500
Tyloxapol	Sigma	Cat# T8761-50G
Dimethyl sulfoxide (DMSO)	Sigma	Cat# D8418-100ML
Recombinant human IL-7	R&D Systems	Cat# 207-IL
Recombinant human IL-2	Peptotech	Cat# 200-02
Recombinant human IFN $\gamma$	ThermoFisher Scientific	Cat# RIFNG50
Recombinant mouse IL-2	R&D Systems	Cat# 402-ML-100
Recombinant 2C12 NKT TCR	This paper	N/A
Recombinant mouse CD1d (mCD1d)	This paper	N/A
HisPur™ Ni-NTA affinity resin	ThermoFisher Scientific	Cat# 88223
Superdex 200 16/60 size exclusion column	GE Healthcare	Cat# 28989335
MonoQ GL anion exchange column	GE Healthcare	Cat# 17-5166-01
PEG 3350	Sigma-Aldrich	Cat# 202444

(Continued on next page)

**Continued**

REAGENT or RESOURCE	SOURCE	IDENTIFIER
Taccimate	Hampton Research	Cat# HR2-825
Carboxyfluorescein succinimidyl ester (CFSE)	ThermoFisher Scientific	Cat# C34554
Mouse CD1d tetramer, $\alpha$ GalCer-loaded	This paper	N/A
<b>Critical Commercial Assays</b>		
Mouse CBA Th1/Th2/Th17 Cytokine kit	BD Biosciences	Cat# 560485
<b>Deposited Data</b>		
Crystal structure 2C12 TCR-CD1d-AH10-7	This paper –structure deposited	PDB code: 6BNL
Crystal structure 2C12 TCR-CD1d- $\alpha$ -GalCer	This paper – structure deposited	PDB code: 6BNK
Crystal structure mouse CD1d-NU-alpha-GalCer-iNKT TCR complex	<a href="#">Aspeshlagh et al., 2011</a>	PDB code: 3QUZ
Crystal structure human NKT TCR-CD1d-4' deoxy-alpha-galactosylceramide ternary complex	<a href="#">Wun et al., 2012</a>	PDB code: 3VWK
Crystal structure of CD1d-lipid-antigen complexed with Beta-2-Microglobulin, NKT15 Alpha-Chain and NKT15 Beta-Chain	<a href="#">Borg et al., 2007</a>	PDB code: 2PO6
Structure of the mouse CD1d-4CIPhC-alpha-GalCer-iNKT TCR complex	<a href="#">Aspeshlagh et al., 2013</a>	PDB code: 4IRJ
<b>Experimental Models: Cell Lines</b>		
SF9 insect cells	ThermoFisher Scientific	Cat# 12659017
HighFive™ insect cells	ThermoFisher Scientific	Cat# B85502
DN3A4-1.2 mouse iNKT cell hybridoma	Dr. M. Kronenberg	N/A
BW5147 $\alpha$ - $\beta$ -, mouse thymoma line	Dr. S. Behar, University of Massachusetts, USA	Letourneur F & Malissen B. Eur J Immunol. 1989 Dec;19(12):2269-74.
HeLa cells, hCD1d transfected	<a href="#">Spada et al., 2000</a>	N/A
Human iNKT cell clone HDD5	<a href="#">Bricard et al., 2009</a>	N/A
Human iNKT cell clone HDD3	<a href="#">Bricard et al., 2009</a>	N/A
B16-F10 mouse melanoma	ATCC	ATCC CRL-6475
JAWS II mouse dendritic cell line	ATCC	ATCC CRL-11904
<b>Experimental Models: Organisms/Strains</b>		
Mouse: C57BL/6 J	JAX	Stock# 000664
Mouse: hCD1d-KI (C57BL/6 J background)	<a href="#">Wen et al., 2013</a>	N/A
<b>Recombinant DNA</b>		
2C12 TCR $\alpha$ - and $\beta$ - chains plasmids in pET30	From Daniel G. Pellicci (University of Melbourne)	N/A
Mouse CD1d/ $\beta$ 2m plasmid	<a href="#">Pellicci et al., 2009</a>	N/A
<b>Software and Algorithms</b>		
Glide	Schrodinger Suite 2016-3	<a href="https://www.schrodinger.com/">https://www.schrodinger.com/</a>
Qsite	Schrodinger Suite 2016-3	<a href="https://www.schrodinger.com/">https://www.schrodinger.com/</a>
Maestro (image rendering) version 10.6.014	Schrodinger Suite 2016-3	<a href="https://www.schrodinger.com/">https://www.schrodinger.com/</a>
iMOSFLM and SCALA	Ccp4 suite	<a href="http://www.mrc-lmb.cam.ac.uk/harry/imosflm/index.html">http://www.mrc-lmb.cam.ac.uk/harry/imosflm/index.html</a>
PHASER	<a href="#">McCoy et al., 2007</a>	<a href="https://www.phenix-online.org/">https://www.phenix-online.org/</a>
COOT	<a href="#">Emsley et al., 2010</a>	<a href="https://www2.mrc-lmb.cam.ac.uk/personal/pemsley/coot/">https://www2.mrc-lmb.cam.ac.uk/personal/pemsley/coot/</a>
BUSTER 2.10	<a href="#">Smart et al., 2012</a>	<a href="https://www.globalphasing.com/buster/">https://www.globalphasing.com/buster/</a>
PYMOL	The PyMOL Molecular Graphics System, Version 2.0 Schrödinger, LLC.	<a href="https://pymol.org/2/">https://pymol.org/2/</a>
BIAevaluation 3.1	Biacore AB	<a href="https://www.biacore.com/lifesciences/service/downloads/software_licenses/biaevaluation/">https://www.biacore.com/lifesciences/service/downloads/software_licenses/biaevaluation/</a>
GraphPad Prism 7.0	GraphPad	<a href="https://www.graphpad.com/">https://www.graphpad.com/</a>
FlowJo, version 10.4	Tree Star, Inc.	<a href="https://www.flowjo.com/">https://www.flowjo.com/</a>

## CONTACT FOR REAGENT AND RESOURCE SHARING

Further information and requests for resources and reagents should be directed to and will be fulfilled by the Lead Contact, Amy R. Howell ([amy.howell@uconn.edu](mailto:amy.howell@uconn.edu)).

## EXPERIMENTAL MODEL AND SUBJECT DETAILS

### Animals

C57BL/6 mice were purchased from Jackson Laboratory, and hCD1dKI mice were bred and maintained in the animal facilities of the Albert Einstein College of Medicine and the University of Southern California Keck School of Medicine. Animals were maintained according to the guidelines of the Association for Assessment and Accreditation of Laboratory Animal Care. Female mice between 6–8 weeks of age were used for all studies and were housed under standard specific pathogen-free conditions. Animals were randomly assigned to experimental groups. The influence of sex or gender on the results of the experiments in this study has not been assessed. All studies involving mice were specifically approved by the Institutional Animal Care and Use Committees (IACUCs) of the Albert Einstein College of Medicine and the University of Southern California Keck School of Medicine.

### Human Subjects

Adult peripheral human blood samples were obtained from the Australian Red Cross Blood Service under agreement number 13-04VIC-07. Three female donors (ages 16, 35 and 74 years) and one male donor (age 68 years) were studied. The influence of sex or gender on the results of the experiments in this study has not been assessed. Informed consent for blood donation was obtained from all subjects.

### Cell Lines and Primary Cell Cultures

The mouse *i*NKT hybridoma DN3A4-1.2 was obtained from Dr. Mitchell Kronenberg (La Jolla Institute for Allergy and Immunology, San Diego, CA). Hybridoma lines from female wild type or human CD1d knock-in mice were produced by fusion of purified splenic *i*NKT cells with mouse thymoma line BW5147 $\alpha^{-}\beta^{-}$  using standard methods as previously described (Johnson et al., 2017). BMDCs from 6–8 week old female C57BL/6 mice (Jackson Laboratories) and from hCD1dKI mice bred in our facilities were generated and cultured as described previously (Arora et al., 2014). Human *i*NKT clones HDD3 and HDD5 were established from PBMCs of anonymous normal human donors as described and were cultured at 37°C in a 5% CO<sub>2</sub> incubator in RPMI-1640 medium with 10% human serum, recombinant human IL-2 and IL-7 (Bricard et al., 2010). The JAWS II cell line (derived from C57BL/6.p53<sup>-/-</sup> mice) was obtained from the American Type Culture Collection (ATCC) and was cultured at 37°C in a 5% CO<sub>2</sub> incubator in  $\alpha$ -MEM medium supplemented with 20% fetal calf serum (Atlanta Biologicals), 10 mM HEPES, 50  $\mu$ M  $\beta$ -mercaptoethanol, 50  $\mu$ g/mL gentamicin, 100 ng/mL GM-CSF (Peprotech), 0.1 mM of nonessential amino acids (NEAA) and essential amino acids (EAA). The B16-F10 mouse melanoma cell line was obtained from the ATCC and maintained as a cryopreserved stock expanded by three passages. The identities of cell lines were not validated for this study.

For *in vitro* proliferation and *i*NKT cell expansion assays, human peripheral blood mononuclear cells (PBMCs) were labeled with 2  $\mu$ M carboxyfluorescein diacetate succinimidyl ester (CFSE) at 37°C for 10 minutes. Labeled cells were then cultured in culture media with graded doses of glycolipid antigens for 7 days in the presence of 50 U/mL human IL-2. Cultures were kept at 37°C in an incubator containing 5% CO<sub>2</sub>. Cells were harvested at the end of culture, labeled by staining with fluorescently labeled anti-CD3 mAb and  $\alpha$ -GalCer loaded hCD1d tetramers, and analyzed for proliferating cells through generational dye divisions via flow cytometry.

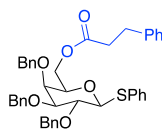
## METHOD DETAILS

### Glycolipid Synthesis

KRN7000 is commercially available (Avanti Polar Lipids). The syntheses of AH03-1 and DB03-4 have been previously reported (Ndonye et al., 2005; Yu et al., 2005). All chemicals, solvents and deuterated solvents were purchased from Sigma-Aldrich, Alfa-Aesar, Oakwood Chemicals or Fisher Scientific and used as received unless noted. Methylene chloride (DCM) was dried over CaH<sub>2</sub>. Deuterated chloroform (CDCl<sub>3</sub>) was dried over activated 4 Å molecular sieves. All reactions, unless specified, were conducted under an atmosphere of N<sub>2</sub> in glassware that had been oven or flame dried. <sup>1</sup>H NMR spectra were recorded at 400 MHz and/or at 500 MHz and calibrated to the residual CHCl<sub>3</sub> peak at 7.27 ppm. <sup>13</sup>C NMR spectra were recorded at 100 MHz and/or at 125 MHz and calibrated to the CDCl<sub>3</sub> peak at 77.23 ppm. Chemical shifts are reported in units of parts per million (ppm). Infrared (IR) spectra were recorded on an FT-IR spectrophotometer and are reported in cm<sup>-1</sup>. High-resolution mass spectra were obtained on an AccuTOF instrument at the University of Connecticut. Specific rotations [ $\alpha$ ]<sub>D</sub> were obtained on a JASCO P-2000 polarimeter, using the sodium D-line as a source, and the concentration (c) is expressed in g per 100 mL. Flash chromatography was performed on silica gel, 40 microns, 32–63 flash silica. Thin layer chromatography was performed on silica gel (silica gel 60 F<sub>254</sub>) glass plates, and the compounds were visualized by UV and/or 5% phosphomolybdic acid in ethanol. Proton and carbon NMR spectra of purified intermediates, AH10-7 and AH15-1 are available as [Data S1](#).



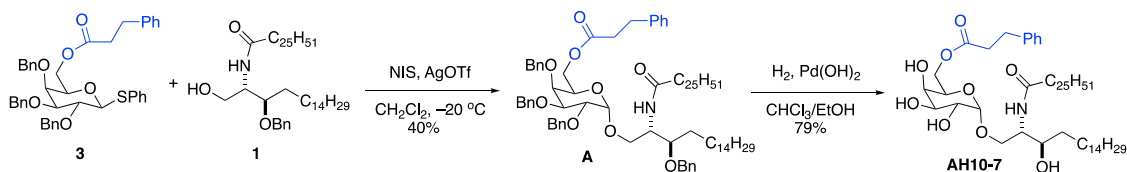
## Synthesis and Characterization of AH10-7 and AH15-1



### Phenyl 2,3,4-Tri-O-benzyl-6-hydrocinnamoyl-1-thio-β-D-galactopyranoside (**3**)

Hydrocinnamic acid (0.59 g, 3.9 mmol), *N,N'*-dicyclohexylcarbodiimide (DCC) (0.76 g, 3.7 mmol) and *N,N*-dimethylaminopyridine (DMAP) (0.087 g, 0.71 mmol) were added to a solution of phenyl 2,3,4-tri-*O*-benzyl-1-thio-β-D-galactopyranoside (Bourgeaux and Combret, 2000; Ziegler et al., 1999) (1.93 g, 3.56 mmol) in DCM (20 mL). The solution was then stirred at rt for 24 h. The resulting reaction mixture was concentrated and purified by flash chromatography on silica gel (petroleum ether/EtOAc, 85:15) to afford **3** as a white solid (1.47 g, 61%): mp 66–68°C;  $[\alpha]_D^{22}$  –23.2 (c 1.78, DCM); IR (neat) 3026, 2926, 2864, 1721, 1452, 733 cm<sup>-1</sup>; <sup>1</sup>H NMR (400 MHz, CDCl<sub>3</sub>) δ 7.65–7.62 (m, 2H), 7.47–7.23 (m, 23H), 5.03 (d, *J* = 11.5 Hz, 1H), 4.89 (d, *J* = 10.2 Hz, 1H), 4.86–4.78 (m, 3H), 4.67 (d, *J* = 9.6 Hz, 1H), 4.65 (d, *J* = 11.5 Hz, 1H), 4.34 (dd, *J* = 11.2, 6.9 Hz, 1H), 4.20 (dd, *J* = 11.2, 5.6 Hz, 1H), 4.01 (dd, *J* = 9.4, 9.4 Hz, 1H), 3.83 (d, *J* = 2.0 Hz, 1H), 3.63 (dd, *J* = 9.2, 2.5 Hz, 1H), 3.58 (dd, *J* = 6.2, 6.2 Hz, 1H), 2.97 (t, *J* = 7.7 Hz, 2H), 2.64 (t, *J* = 7.9 Hz, 2H); <sup>13</sup>C NMR (100 MHz, CDCl<sub>3</sub>) δ 172.5, 140.4, 138.4, 138.4, 138.3, 134.1, 131.9, 128.9, 128.6, 128.5, 128.4, 128.4, 128.2, 127.9, 127.8, 127.7, 127.4, 126.5, 87.9, 84.3, 77.5, 76.2, 75.8, 74.4, 73.6, 73.3, 63.5, 35.7, 30.9; HRMS (ESI) calculated for C<sub>42</sub>H<sub>46</sub>NO<sub>6</sub>S (M + NH<sub>4</sub>)<sup>+</sup> *m/z*: 692.3046, found: 692.3037.

### Scheme 1. Synthesis of AH10-7



### (2*S*,3*R*)-3-*O*-Benzyl-1-*O*-(2,3,4-tri-*O*-benzyl-6-hydrocinnamoyl-α-*D*-galactopyranosyl)-2-(*N*-hexacosanoylamino)octadecan-1,3-diol (**A**)

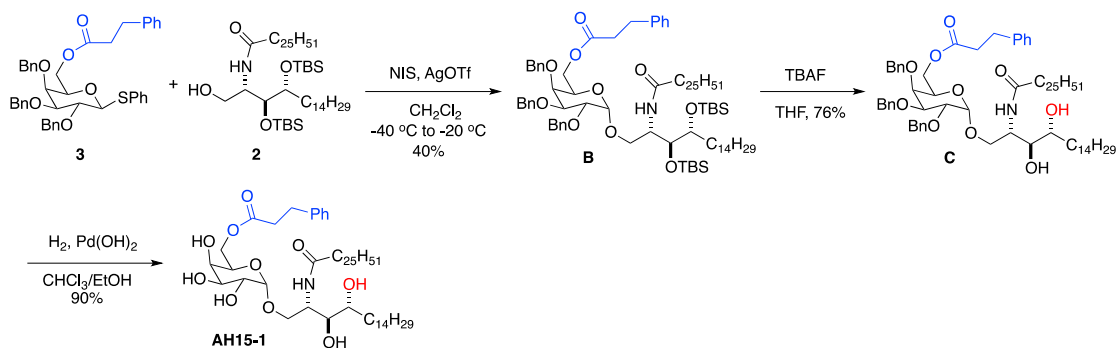
Phenyl 2,3,4-tri-*O*-benzyl-6-hydrocinnamoyl-1-thio-β-D-galactopyranoside (**3**) (100 mg, 0.148 mmol) and (2*S*,3*R*)-3-*O*-benzyl-2-(*N*-hexacosanoylamino)octadecan-1,3-diol (**1**) (Ndonye et al., 2005) (137 mg, 0.177 mmol) were dried by azeotroping with toluene (3 X 10 mL). The mixture was dissolved in DCM (4 mL), and freshly ground 4 Å MS (50 mg) were added. The mixture was cooled to –20°C, and *N*-iodosuccinimide (43.0 mg, 0.192 mmol) and silver triflate (12.6 mg, 0.0488 mmol) were added. The solution was stirred at –20°C until **3** was consumed (based on TLC). The mixture was then stirred an additional 10–20 min at –20°C, followed by the addition of Et<sub>3</sub>N (2 mL). The reaction mixture was diluted with DCM (20 mL) and filtered through Celite. The filtrate was concentrated. Purification by flash chromatography on silica gel (petroleum ether/EtOAc, 90:10) afforded **A** as a sticky solid (79 mg, 40%):  $[\alpha]_D^{21}$  +28.9 (c 2.97, DCM); IR (neat) 3305, 2917, 2849, 1730, 1639, 1467, 1053, 695 cm<sup>-1</sup>; <sup>1</sup>H NMR (400 MHz, CDCl<sub>3</sub>) δ 7.43–7.14 (m, 25H), 5.80 (d, *J* = 8.7 Hz, 1H), 4.97 (d, *J* = 11.4 Hz, 1H), 4.91–4.73 (m, 4H), 4.67 (d, *J* = 11.8 Hz, 1H), 4.59 (d, *J* = 11.4 Hz, 1H), 4.58 (d, *J* = 11.6 Hz, 1H), 4.46 (d, *J* = 11.6 Hz, 1H), 4.28–4.22 (m, 1H), 4.17 (dd, *J* = 11.2, 6.9 Hz, 1H), 4.09–4.05 (m, 2H), 3.92–3.87 (m, 2H), 3.82 (m, 1H), 3.79–3.72 (m, 2H), 3.59 (ddd, *J* = 11.5, 5.8, 5.8 Hz, 1H), 2.92 (t, *J* = 7.8 Hz, 2H), 2.58 (t, *J* = 8.4 Hz, 2H), 2.09–1.95 (m, 2H), 1.57–1.54 (m, 4H), 1.28 (m, 70H), 0.92 (t, *J* = 6.5 Hz, 3H), 0.92 (t, *J* = 6.5 Hz, 3H); <sup>13</sup>C NMR (100 MHz, CDCl<sub>3</sub>) δ 172.9, 172.5, 140.5, 138.8, 138.6, 138.4, 128.7, 128.6, 128.6, 128.5, 128.4, 128.0, 128.0, 127.9, 127.8, 127.6, 127.6, 126.5, 99.1, 79.1, 78.9, 76.8, 74.8, 73.6, 73.5, 72.3, 69.1, 67.8, 63.6, 51.5, 37.0, 35.7, 32.1, 31.1, 31.0, 30.1, 29.9, 29.8, 29.7, 29.6, 25.9, 25.5, 22.9, 14.3; HRMS (ESI) calculated for C<sub>87</sub>H<sub>132</sub>NO<sub>9</sub> (M + H)<sup>+</sup> *m/z*: 1334.9902, found: 1334.9917.

### (2*S*,3*R*)-1-*O*-(6-Hydrocinnamoyl-α-*D*-galactopyranosyl)-2-(*N*-hexacosanoylamino)octadecane-1,3-diol (**AH10-7**)

(2*S*,3*R*)-3-*O*-Benzyl-1-*O*-(2,3,4-tri-*O*-benzyl-6-hydrocinnamoyl-α-*D*-galactopyranosyl)-2-(*N*-hexacosanoylamino)octadecan-1,3-diol (**A**) (14 mg, 0.010 mmol) was dissolved in a 1:1 mixture of EtOH (3.1 mL) and CHCl<sub>3</sub> (3.1 mL). Pd(OH)<sub>2</sub> (20% on carbon, 50.0 mg) was added, and vigorous stirring under H<sub>2</sub> was continued for 24 h. The mixture was filtered through Celite, and the filter cake was washed with CHCl<sub>3</sub>/MeOH (9:1). The filtrate was concentrated, and the residue was purified by gravity chromatography on silica gel (DCM/MeOH, 100:0 to 90:10) to give **AH10-7** as a white solid (8 mg, 79%): mp 123°C;  $[\alpha]_D^{22}$  –0.38 (c 1.0, CHCl<sub>3</sub>/MeOH, 9:1); IR (KBr) 3433, 2920, 1728, 1644 cm<sup>-1</sup>; <sup>1</sup>H NMR (400 MHz, CDCl<sub>3</sub>/CD<sub>3</sub>OD, 80:20) δ 7.09–7.06 (m, 2H), 7.02–6.97 (m, 3H), 4.65 (d, *J* = 3.6 Hz, 1H), 4.05–4.03 (m, 2H), 3.74–3.69 (m, 2H), 3.63–3.45 (m, 5H), 3.41–3.38 (m, 1H), 2.74 (t, *J* = 7.6 Hz, 2H),

2.46 (t,  $J = 8.0$  Hz, 2H), 2.01 (t,  $J = 7.5$  Hz, 2H), 1.42 (m, 2H), 1.31–1.19 (m, 2H), 1.06 (m, 70H), 0.68 (m, 6H);  $^{13}\text{C}$  NMR (100 MHz,  $\text{CDCl}_3/\text{CD}_3\text{OD}$ , 80:20)  $\delta$  174.3, 173.0, 140.1, 128.2, 128.0, 126.1, 99.4, 70.7, 69.7, 69.1, 68.7, 68.3, 67.1, 63.6, 53.3, 36.2, 35.5, 33.8, 31.7, 30.6, 29.4, 29.4, 29.2, 29.1, 25.7, 25.6, 22.4, 13.6; HRMS (FAB) calculated for  $\text{C}_{59}\text{H}_{108}\text{NO}_9$  ( $\text{M} + \text{H}$ ) $^+$   $m/z$ : 974.8019, found: 974.8021.

## Scheme 2. Synthesis of AH15-1



### (2S,3S,4R)-3,4-di-O-tert-butylidimethylsilyl-1-O-(2,3,4-tri-O-benzyl-6-hydrocinnamoyl- $\alpha$ -D-galactopyranosyl)-2-(N-hexacosanoylamino)octadecan-1,3,4-triol (B)

Phenyl 2,3,4-tri-O-benzyl-6-hydrocinnamoyl-1-thio- $\beta$ -D-galactopyranoside (**3**) (124 mg, 0.184 mmol) and (2S,3S,4R)-3,4-di-O-tert-butylidimethylsilyl-2-(N-hexacosanoylamino)octadecan-1,3,4-triol (**2**) (Kim et al., 2004) (342 mg, 0.369 mmol) were dried by azeotroping with toluene (3 X 10 mL). The mixture was dissolved in DCM (3.0 mL), and freshly ground 4 Å MS (50 mg) were added. The mixture was cooled to  $-40^\circ\text{C}$ , and *N*-iodosuccinimide (52 mg, 0.23 mmol) and silver triflate (15 mg, 0.059 mmol) were added. The mixture was stirred at  $-20^\circ\text{C}$  until **3** was consumed (based on TLC). The mixture was then stirred an additional 10–20 min at  $-20^\circ\text{C}$ , followed by the addition of  $\text{Et}_3\text{N}$  (3 mL). The reaction mixture was diluted with DCM (20 mL) and filtered through Celite. The filtrate was concentrated. Purification by flash chromatography on silica gel (petroleum ether/EtOAc, 90:10) afforded **B** as a viscous oil (51 mg, 40%):  $[\alpha]_{\text{D}}^{22} -82.9$  (c 0.5, DCM); IR (neat) 2922, 2852, 1741, 1680, 1047, 832  $\text{cm}^{-1}$ ;  $^1\text{H}$  NMR (400 MHz,  $\text{CDCl}_3$ )  $\delta$  7.42–7.19 (m, 20H), 5.87 (d,  $J = 7.0$  Hz, 1H), 4.94 (d,  $J = 11.4$  Hz, 1H), 4.86 (d,  $J = 3.5$  Hz, 1H), 4.84 (d,  $J = 11.8$  Hz, 1H), 4.82 (d,  $J = 11.7$  Hz, 1H), 4.75 (d,  $J = 11.8$  Hz, 1H), 4.68 (d,  $J = 11.8$  Hz, 1H), 4.55 (d,  $J = 11.4$  Hz, 1H), 4.22–4.17 (m, 1H), 4.14–4.12 (m, 2H), 4.07 (dd,  $J = 10.1$ , 3.5 Hz, 1H), 4.04 (dd,  $J = 9.7$ , 3.6 Hz, 1H), 3.92–3.87 (m, 3H), 3.82 (m, 1H), 3.71–3.67 (m, 2H), 2.92 (t,  $J = 7.7$  Hz, 2H), 2.55 (m, 2H), 2.01 (t,  $J = 7.5$  Hz, 2H), 1.64–1.45 (m, 4H), 1.28 (m, 68H), 0.93 (s, 9H), 0.91 (s, 9H), 0.89 (m, 6H), 0.09 (s, 3H), 0.07 (s, 3H), 0.06 (s, 6H);  $^{13}\text{C}$  NMR (100 MHz,  $\text{CDCl}_3$ )  $\delta$  173.3, 172.3, 140.6, 138.8, 138.7, 138.5, 128.7, 128.6, 128.6, 128.5, 128.4, 128.1, 127.9, 127.9, 127.8, 127.6, 126.5, 99.8, 79.3, 76.7, 76.1, 76.0, 74.8, 74.6, 73.8, 73.4, 68.9, 68.7, 62.8, 51.7, 37.0, 35.7, 33.7, 32.1, 30.9, 30.1, 29.9, 29.8, 29.7, 29.6, 26.3, 26.3, 26.2, 25.9, 22.9, 18.5, 18.4, 14.3,  $-3.5$ ,  $-3.7$ ,  $-4.4$ ,  $-4.6$ ; HRMS (ESI) calculated for  $\text{C}_{92}\text{H}_{154}\text{NO}_{10}\text{Si}_2$  ( $\text{M} + \text{H}$ ) $^+$   $m/z$ : 1489.1111, found: 1489.1168.

### (2S,3S,4R)-1-O-(2,3,4-Tri-O-benzyl-6-hydrocinnamoyl- $\alpha$ -D-galactopyranosyl)-2-(N-hexacosanoylamino)octadecan-1,3,4-triol (C)

Tetrabutylammonium fluoride (TBAF) (1 M in THF, 0.14 mL, 0.14 mmol) was added to a stirred solution of (2S,3S,4R)-3,4-di-O-tert-butylidimethylsilyl-1-O-(2,3,4-tri-O-benzyl-6-hydrocinnamoyl- $\alpha$ -D-galactopyranosyl)-2-(N-hexacosanoylamino)octadecan-1,3,4-triol (**B**) (51 mg, 0.034 mmol) in THF (2.5 mL) at  $0^\circ\text{C}$ . The solution was stirred at  $0^\circ\text{C}$  until the starting material was consumed (based on TLC). The reaction mixture was diluted with saturated  $\text{NH}_4\text{Cl}$  (10 mL) and extracted with DCM (2 X 10 mL). The combined organic layers were dried ( $\text{Na}_2\text{SO}_4$ ) and concentrated. Purification by flash column chromatography on silica gel (petroleum ether/EtOAc 70:30) afforded **C** as an off-white solid (33 mg, 76%): mp  $86\text{--}88^\circ\text{C}$ ;  $[\alpha]_{\text{D}}^{21} +36.8$  (c 1.25, DCM); IR (neat) 3320, 2917, 2850, 1733, 1638, 1046, 695  $\text{cm}^{-1}$ ;  $^1\text{H}$  NMR (400 MHz,  $\text{CDCl}_3$ )  $\delta$  7.43–7.25 (m, 17H), 7.22–7.19 (m, 3H), 6.28 (d,  $J = 8.4$  Hz, 1H), 4.94 (d,  $J = 11.4$  Hz, 1H), 4.89 (d,  $J = 7.9$  Hz, 1H), 4.88 (d,  $J = 7.4$  Hz, 1H), 4.83 (d,  $J = 11.7$  Hz, 1H), 4.79 (d,  $J = 11.7$  Hz, 1H), 4.71 (d,  $J = 11.6$  Hz, 1H), 4.59 (d,  $J = 11.4$  Hz, 1H), 4.28–4.24 (m, 1H), 4.15 (dd,  $J = 11.2$ , 7.0 Hz, 1H), 4.09–4.05 (m, 2H), 3.89–3.78 (m, 5H), 3.60 (br s, 1H), 3.52–3.50 (m, 2H), 2.92 (t,  $J = 7.7$  Hz, 2H), 2.59 (t,  $J = 8.0$  Hz, 2H), 2.23 (br s, 1H), 2.17 (m, 2H), 1.63–1.59 (m, 4H), 1.28 (m, 68H), 0.90 (m, 6H);  $^{13}\text{C}$  NMR (100 MHz,  $\text{CDCl}_3$ )  $\delta$  173.1, 172.8, 140.5, 138.4, 138.2, 137.9, 128.7, 128.6, 128.5, 128.5, 128.3, 128.1, 128.0, 127.7, 126.5, 98.9, 79.5, 76.4, 76.1, 74.8, 74.5, 74.2, 73.5, 73.2, 69.7, 69.0, 63.5, 49.4, 37.0, 35.7, 33.6, 32.1, 30.9, 29.9, 29.8, 29.6, 29.6, 26.1, 26.0, 22.9, 14.3; HRMS (ESI) calculated for  $\text{C}_{80}\text{H}_{126}\text{NO}_{10}$  ( $\text{M} + \text{H}$ ) $^+$   $m/z$ : 1260.9382, found: 1260.9278.

### (2S,3S,4R)-1-O-(6-Hydrocinnamoyl- $\alpha$ -D-galactopyranosyl)-2-(N-hexacosanoylamino)octadecan-3,4-diol (AH15-1)

Pd(OH)<sub>2</sub> (20% on carbon, 96 mg) was added to a stirred solution of (2S,3S,4R)-1-O-(2,3,4-tri-O-benzyl-6-hydrocinnamoyl- $\alpha$ -D-galactopyranosyl)-2-(N-hexacosanoylamino)octadecan-1,3,4-triol (**C**) (33 mg, 0.026 mmol) in EtOH (6 mL) and CHCl<sub>3</sub> (2 mL). The mixture was stirred vigorously under H<sub>2</sub> (1 atm) for 12 h. The reaction mixture was filtered through Celite, and the filter cake was washed with 50:50 CHCl<sub>3</sub>/MeOH. The filtrate was concentrated, and the residue was purified by flash column chromatography on silica gel (CHCl<sub>3</sub>/MeOH, 90:10) to afford **AH15-1** as a white solid (22 mg, 90%): mp 110–112 °C; [ $\alpha$ ]<sub>D</sub><sup>21</sup> +18.2 (c 0.15, DCM/MeOH, 80:20); IR (neat) 3273, 2959, 2915, 2849, 1725, 1642, 1259, 1074, 1015, 794 cm<sup>-1</sup>; <sup>1</sup>H NMR (400 MHz, CDCl<sub>3</sub>/CD<sub>3</sub>OD 80:20)  $\delta$  7.27–7.23 (m, 2H), 7.18–7.12 (m, 3H), 4.87 (d, *J* = 3.6 Hz, 1H), 4.22–4.20 (m, 2H), 4.17–4.15 (m, 1H), 3.90 (dd, *J* = 6.1, 6.1 Hz, 1H), 3.83 (dd, *J* = 10.6, 4.6 Hz, 1H), 3.79–3.73 (m, 2H), 3.69–3.60 (m, 2H), 3.52–3.46 (m, 2H), 2.91 (t, *J* = 7.7 Hz, 2H), 2.63 (t, *J* = 7.9 Hz, 2H), 2.16 (t, *J* = 7.3 Hz, 2H), 1.65–1.51 (m, 4H), 1.23 (br s, 68 H), 0.84 (t, *J* = 6.4 Hz, 3H), 0.84 (t, *J* = 6.4 Hz, 3H); <sup>13</sup>C NMR (125 MHz, CDCl<sub>3</sub>/CD<sub>3</sub>OD, 80:20)  $\delta$  174.1, 173.2, 140.2, 128.4, 128.2, 126.2, 99.5, 74.6, 72.1, 70.0, 69.1, 68.7, 68.4, 67.5, 63.6, 50.0, 36.4, 35.6, 32.5, 31.8, 30.7, 29.7, 29.6, 29.6, 29.6, 29.5, 29.5, 29.3, 29.3, 29.3, 29.3, 25.8, 22.6, 13.9; HRMS (ESI) calculated for C<sub>59</sub>H<sub>108</sub>NO<sub>10</sub> (M + H)<sup>+</sup> *m/z*: 990.7973, found: 990.7990.

### Reconstitution of Glycolipids for *In Vitro* and *In Vivo* Administration

For *in vitro* assays, glycolipid stock solutions were prepared at 100  $\mu$ M in DMSO (Sigma). Immediately before use, these stocks were heated to 70°C, sonicated for 5 min and then diluted to 1  $\mu$ M in pre-warmed (37°C) culture medium (RPMI-1640 with 10% FCS). This stock was further diluted with culture medium immediately before adding to cell cultures to give the desired final glycolipid concentrations ranging from 0.01 - 1000 nM and a final DMSO concentration of  $\leq$  1%. For *in vivo* injection into mice, glycolipids were first dissolved to 20 mM in DMSO and then further diluted to 200  $\mu$ M using PBS + 0.5% Tween-20. This solution was diluted 1:10 with prewarmed (80°C) PBS immediately before injection of mice. Injection of 200  $\mu$ l delivered 4 nmol of glycolipid in a vehicle with final composition of PBS + 0.1% DMSO + 0.05% Tween-20.

### CD1d Tetramer Preparation

The cDNA sequences encoding human  $\beta$ 2-microglobulin (encoding amino acids IQRTP to RDMGS) and the extracellular domains of human CD1d (encoding amino acids VPQRL to VLYWGS and C-terminal BirA and hexahistidine tags (amino acid sequence GLNDIFEAQKIEWHEHHHHHH)) were cloned into the expression vector pHLsec and transfected into mammalian HEK-293S.GnTI cells. The expressed soluble hCD1d/ $\beta$ 2M protein complexes were purified from the culture supernatant using Nickel agarose affinity columns and biotinylated using BirA-specific biotin ligase enzyme. Biotinylated CD1d was loaded with  $\alpha$ -GalCer PBS-44 provided by Paul Savage (Brigham Young University) and converted to fluorescent tetramers by the addition of phycoerythrin (PE)-conjugated streptavidin (BD Biosciences).

### *In Vitro* and *In Vivo* Activation of *i*NKT Cells

Mouse *i*NKT hybridoma lines were stimulated using standard conditions with mouse BMDCs as APCs, and supernatants were harvested after 18 h for determination of levels of IL-2 by capture ELISA (Im et al., 2009). Human *i*NKT cell lines were co-cultured in 96 well plates at 2 x 10<sup>4</sup> cells/well with APCs (2 x 10<sup>4</sup>/well hCD1d-transfected HeLa cells or monocyte-derived DCs) in 100  $\mu$ L of RPMI-1640 supplemented with 10% human serum, 30 U/mL IL-2 and 10 ng/mL IL-7 at 37°C (Spada et al., 2000). Glycolipid antigens were added at concentrations ranging from 0.1 - 1000 nM. Supernatants were harvested after 18 h of culture, and concentrations of human IFN $\gamma$  were measured by capture ELISA as described (Bricard et al., 2010; Im et al., 2009). For *in vivo* stimulation of *i*NKT cells, C57BL/6 and hCD1dKI mice were injected i.v. via the retro-orbital plexus with 4 nmol of glycolipids. Mice were bled 2 h and 24 h later, and serum samples were stored at -80°C before cytokine measurement by cytometric bead array (BD Biosciences) according to instructions provided with the assay kit.

### Lipid Raft Localization of CD1d/Glycolipid Complexes

The method used for estimating lipid raft localization by detergent sensitivity has been described previously in detail (Arora et al., 2011). Briefly, JAWS II cells were seeded at a density of 2.5 x 10<sup>5</sup> cells per well in 100  $\mu$ l culture media in flat bottom 96 well plates. Glycolipids were added to a final concentration of 200 nM. As an inert vehicle control, the cells were cultured in medium containing only 0.02% DMSO. After 16 h of culture, the cells were detached, washed 3 times and resuspended in 50  $\mu$ l of FACS buffer (PBS + 1% FCS + 0.05% sodium azide) and stained with 5  $\mu$ g/mL of the mCD1d/ $\alpha$ -GalCer complex-specific mAb L363, which was produced and conjugated with Alexa Fluor 647 as previously reported (Yu et al., 2007). For estimation of lipid raft residency, the FACS analysis was performed in a kinetic mode. Triton X-100 was added to a final concentration of 0.06%, and fluorescence intensities were monitored before and after the addition of Triton X-100 for 30s. Data were collected as flow cytometry standard (FCS) files and analyzed using FlowJo software (Tree Star Inc.). MFI values at time 0 (prior to addition of Tx-100) were normalized to 100%, and the relative decrease in MFI values for different agonists after addition of Tx-100 were compared.

### Determination of B16-F10 Melanoma Lung Metastases

B16-F10 metastasis assays were performed as previously described (Schmiege et al., 2003; Wen et al., 2013). Briefly, C57BL/6 mice and hCD1dKI mice (6-8 weeks old, female) were injected i.v. with 4 x 10<sup>5</sup> B16-F10 melanoma cells in 200  $\mu$ l 2-3 days after

administration of 4 nmol i.v. of KRN7000 or AH10-7. Two weeks after challenge, mice were sacrificed, lungs removed, and the numbers of melanized nodules per lung visible under low magnification (10X) were counted.

### Expression and Purification of Mouse CD1d and 2C12 $\alpha\beta$ TCR Proteins

Mouse CD1d associated with  $\beta$ 2-microglobulin ( $\beta$ 2m) was expressed and purified as reported previously (Pellicci et al., 2009). In brief, the mouse CD1d/ $\beta$ 2m construct harboring BirA and Histidine affinity tags was cloned into the pFastBac™ plasmid. The recombinant Bacmid was then amplified in SF9 insect cells and subsequently used to transfect HighFive™ (Hi5) insect cells. The secreted mouse protein was purified by Ni-NTA affinity chromatography (HisPur™-Thermo Scientific), followed by size exclusion chromatography. The 2C12  $\alpha\beta$  TCR construct was kindly provided by Daniel G. Pellicci (University of Melbourne, Australia), and the 2C12 TCR protein was expressed in *E. coli* and purified as inclusion bodies. The refolding and purification procedures for the soluble 2C12 TCR were based on previously described methods (Garboczi et al., 1996). In brief, a total of 120 mg and 144 mg of the 2C12 TCR  $\alpha$ - and  $\beta$ -chains, respectively, were injected drop wise to a 1 L pre-cooled refolding buffer composed of 100 mM Tris-pH 8.0, 2 mM NaEDTA, 5 M urea, 0.4 M L-arginine, 0.5 M oxidized glutathione, 5 mM reduced glutathione, 0.8 mM PMSF. Two injections were performed 8 h apart, and the refolding mixture was stirred overnight at 4°C and then dialysed against 10 mM Tris-pH 8.0. The refolding solution was then loaded onto a diethylaminoethyl (DEAE) weak anion exchange chromatography column whereby the 2C12 TCR was eluted with 30 mL of elution buffer containing 10 mM Tris-pH 8.0 and 270 mM NaCl. The eluent was concentrated to 5 mL using an Amicon Ultra Centrifugal concentrator with a 30 KDa cutoff (Millipore) and loaded onto a size exclusion chromatography column (GE Healthcare) pre-equilibrated with 10 mM Tris-pH 8.0, 150 mM NaCl. Fractions containing the 2C12 TCR were further purified by anion exchange (HiTrap™ Q HP column – GE Healthcare) and hydrophobic interaction (HiTrap™ Phenyl HP column - GE Healthcare) chromatography techniques.

### Glycolipid Loading of mCD1d and Purification of Ternary Complexes

Glycolipids solutions of AH10-7 and KRN7000 at 1 mg/mL in PBS with 0.5% tyloxapol and 2.5% DMSO were sonicated for 20 min and immediately transferred to a 60°C water bath for 1 min. The lipids were then added directly to mCD1d at molar ratios ranging from 3:1 to 10:1 and incubated at room temperature for 15 h. The loaded proteins were then purified by anion exchange chromatography (MonoQ). The formation of the 2C12 TCR-mCD1d-Ag complex was achieved by mixing the desired glycolipid-loaded mCD1d and the 2C12 TCR at a 1:1 molar ratio in a buffer containing 10 mM Tris-pH 8.0, 150 mM NaCl and incubating on ice for 2 h. The ternary complex was then purified by size exclusion chromatography using a Superdex 200 gel filtration column (GE Healthcare).

### Surface Plasmon Resonance

The affinities between the 2C12 TCR and mCD1d loaded with AH10-7 or KRN7000 were measured by surface plasmon resonance (SPR) using a Biacore3000 (GE Healthcare). The glycolipid-loaded mCD1d was biotinylated and passed over a streptavidin (SA)-coated chip in HBS buffer (150 mM NaCl, 10 mM HEPES, pH 7.4) to capture ~3000 response units (RU) of biotinylated protein to the chip surface. A series of concentrations of the 2C12 TCR ranging from 0 to 50  $\mu$ M in HBS buffer at 25°C was used to examine the affinity for mCD1d-glycolipid complexes. The specific response was determined by subtracting the response of a flow cell coated by streptavidin or by mCD1d loaded with endogenous lipids. The BIAevaluation 3.1 software (Biacore AB) was used to estimate the steady-state  $K_d$  values, and the Prism program was used for statistical analysis, curve fitting and graphic presentation.

### X-ray Crystallography

Crystals of the 2C12 TCR-mCD1d-AH10-7 and 2C12 TCR-mCD1d-KRN7000 ternary complexes were grown in hanging drops containing 5 mg/mL protein at 4°C in 18-20% PEG 3350, 8% Tacsimate pH 5.0 and 0.5% dioxane. The crystals were flash-frozen and data were collected at the Australian Synchrotron (MX2 beamline). The data were processed with the program iMOSFLM and were scaled with SCALA from the CCP4 suite of programs (Winn et al., 2011). Molecular replacement was carried out with the program PHASER (McCoy, 2007; McCoy et al., 2007) and using the mouse CD1d and the  $\alpha\beta$  TCR from the ternary complex structure (PDB code: 3QUZ) as independent search ensembles. Iterative model improvement and refinement cycles were performed with the programs COOT (Emsley et al., 2010) and BUSTER 2.10 (Bricogne et al., 2017), respectively. The quality of the structures was validated at the Research Collaboratory for Structural Bioinformatics Protein Data Bank Data (RCSB PDB), and deposited in the PDB database with ID codes 6BNL (2C12 TCR-CD1d-AH10-7) and 6BNK (2C12 TCR-CD1d-KRN7000). Visual representations were generated using MacPyMOL (PyMOL Molecular Graphics System, Version 2.0 Schrödinger, LLC. <http://www.pymol.org>).

### Computational Methods

For the docking experiments, the mCD1d-TCR and hCD1d-TCR complexes from PDB files 6BNL and 3VWK, respectively, were prepared (e.g., H atoms added, protonation and tautomeric states assigned, and H-bond donor/acceptor groups reoriented) with the Protein Preparation application in Maestro version 10.6.014 (Sastry et al., 2013). In order to have all-atom models of the binding site, the unresolved side chain of CD1d-Lys65 in PDB 6BNL was reconstructed by superimposing the backbone of CD1d from a previous crystal structure (PDB 4IRJ) with the similarly bound C6"-modified  $\alpha$ -GalCer AH10-7. Semi-flexible docking was performed with standard precision Glide (Halgren et al., 2004). The galactose and glycosidic linkage were treated flexibly, while torsions along

the sphingoid base and fatty acid chains were fixed to the crystallographic values. Because sphinganine- and phytosphingosine-containing ceramides experimentally have different chain conformations in the CD1d binding groove, docked ligands were derived from CD1d-TCR crystal structures loaded with each of these types of ligands.

For docking into mCD1d-TCR, AH10-7 was taken from PDB 6BNL, and AH03-1 was prepared by replacing the C6''-hydrocinnamoyl substituent of AH10-7 with a hydroxyl. The phytosphingosine-containing AH15-1 was derived from Nu- $\alpha$ -GalCer, because PDB 3QUZ is the highest resolution crystal structure of a C6''-modified phytosphingosine-based ligand available. KRN7000 was built from AH15-1 by replacement of the C6''-substituent in the same manner that AH03-1 was prepared from AH10-7. For docking into hCD1d-TCR, AH03-1 was prepared from the 4',4''-dideoxy analogue of KRN7000 present in the PDB 3VWK crystal structure by adding the C4''-OH of the galactose. AH10-7 was then prepared by replacing the C6''-OH with the hydrocinnamoyl group. KRN7000 was taken from PDB 2PO6, and as with AH10-7, AH15-1 was prepared by substituting the hydrocinnamoyl group for the C6''-OH. Eight rotamers for each ligand were generated by varying the orientation of the C3''- and C4''-OH groups. These rotamers were docked, and the top ten poses for each submitted structure were conformationally clustered into distinct poses.

Using the highest ranked docking poses from Glide, we performed QM/MM calculations of all complexes containing mouse or human CD1d with optimization of only the glycolipid ligands (Duff et al., 2011). B3LYP/6-31g\* was used for the QM region (ligands) and the OPLS-AA force field for the rest of the protein as implemented in Qsite (Schrodinger Inc.) (Murphy et al., 2000). Binding energies were modeled by subtracting from the QM/MM energy the MM energy of the apo-protein (CD1d-TCR) and the minimized energy of the ligand in octanol. The Poisson-Boltzmann method was used for implicit solvent calculations (Tannor et al., 1994).

### QUANTIFICATION AND STATISTICAL ANALYSIS

Data are shown as mean values with error bars representing one standard error (SE). Levels of significance were  $P < 0.05$  (\*),  $P < 0.01$  (\*\*),  $P < 0.001$  (\*\*\*),  $P < 0.0001$  (\*\*\*\*). Statistical analyses were done using GraphPad Prism software. Data with multiple groups were analyzed for overall significance using one-way ANOVA, and level of significance for pairwise comparisons of selected groups was calculated using Dunnett post-test. Group sizes (n) for individual experiments are defined in the figure legends.

### DATA AND SOFTWARE AVAILABILITY

The structures of the NKT 2C12 TCR-CD1d-KRN7000 and NKT 2C12 TCR-CD1d-AH10-7 ternary complexes were deposited in the RCSB Protein Data Bank (PDB) under the accession codes 6BNK and 6BNL, respectively.